Linkages of surface air temperature variations over Central Asia with large-scale climate patterns

Yuanhuang Zhuang
Institute of Atmospheric Physics, Chinese Academy of Sciences
Jingyong Zhang (zjy@mail.iap.ac.cn)
Institute of Atmospheric Physics Chinese Academy of Sciences https://orcid.org/0000-0003-1056-8436
Lingyun Wu
Institute of Atmospheric Physics, Chinese Academy of Sciences

Research Article

Keywords: surface air temperature, variations, Central Asia, CSAT, WSAT, SCAND, NAO, AO

Posted Date: March 3rd, 2021

DOI: https://doi.org/10.21203/rs.3.rs-261105/v1

Version of Record: A version of this preprint was published at Theoretical and Applied Climatology on April 24th, 2021. See the published version at https://doi.org/10.1007/s00704-021-03626-9.

Abstract

In this study, we investigate the dominant modes of surface air temperature variations of the cold season (from November through to the next March) and the warm season (from May to September) over Central Asia, and their associations with large-scale climate patterns for the period of 1979–2016. The first two modes of the cold-season surface air temperature (CSAT) over Central Asia, obtained by empirical orthogonal function (EOF) analysis, feature the mono-pole structure and the north-south dipole pattern, respectively. For the warm-season surface air temperature (WSAT), the leading two EOF modes are characterized by the homogenous structure and the northwest-southeast seesaw pattern, respectively. Further analysis indicates that the large-scale atmospheric circulation anomalies play key roles in the CSAT and WSAT variations over Central Asia. The CSAT variation over Central Asia is closely related with the Scandinavia pattern (SCAND), the Arctic Oscillation (AO) and the North Atlantic Oscillation (NAO), while the WSAT variation is tightly tied to the East Atlantic/Western Russia pattern (EAWR) and the NAO. These large-scale climate patterns tend to cause the CSAT and WSAT anomalies over Central Asia via their effects on regional geopotential heights, warming advections and other processes. Our findings are expected to facilitate the improvement of understanding and predicting the CSAT and WSAT variations over Central Asia.

1. Introduction

About 65 million people live in Central Asia, which is a key region connecting Asia and Europe. Due to fragile ecological environment, Central Asia is extremely sensitive to climate change (Lioubimtseva and Henebry 2009; Huang et al. 2017). Surface air temperature (SAT) is one of the most important climate variables, and its anomalies have profound impacts on natural ecology and society over Central Asia and many other regions of the globe (IPCC 2013). Understanding the spatiotemporal changes in SAT over Central Asia are of great significance to the policymaking of climate change adaptation strategy. Previous studies demonstrated that the SAT over Central Asia has been significantly increasing since the beginning of the 20th century, faster than the global warming (Lioubimtseva et al. 2005; Zhang et al. 2010; Hu et al. 2014; Chen et al. 2017). Compared with Springtime, Summertime and Autumntime, the warming of Wintertime is the strongest. The EOF analysis showed that the annual and seasonal average SAT variations over Central Asia is characterized by same-sign pattern, followed by the dipole type in East-West or North-South (Wang et al. 2008; Chen et al. 2009; Zhang et al. 2018; Zhu et al. 2020). Large-scale climate patterns such as the Arctic Oscillation (AO), the North Atlantic Oscillation (NAO), and the Scandinavia pattern (SCAND) have been shown to play a vital role in influencing the climate variations in Eurasia (Barnston and Livezey 1987; Hurrell and Van Loon 1997; Thompson and Wallace 1998, 2000; Steinbrecht et al. 2001; Besselaar et al. 2010; Hoy et al. 2013; Guo and Li 2016; Wang et al. 2016; Hu et al. 2017; Zhuang et al. 2018; Chen et al. 2018, 2019). The importance of a specific large-scale climate pattern to the climate variation depends on the region and the season. For example, it is widely recognized that the El Niño-Southern Oscillation (ENSO) has a significant impact on the East Asian summer monsoon system (Yang and Lau 1998; Wu et al. 2009; Ren et al. 2015; Zhang et al. 2016;

Santoso et al. 2017). Wu et al. (2010) indicated that the summer SAT over Northeast China (NEC) tends to be anomalously lower (higher) than normal in El Niño (La Niña) developing years before the mid-1970s, whereas in 1980s and 1990s, their relationship is weakened or even becomes opposite. The positive phase of the NAO or AO tends to cause warm SAT anomalies over large parts of north Eurasia, and cool SAT anomalies over southern Europe and the Middle East during winter (Gong et al. 2001; Wu and Wang 2002; Li and Wang 2013; Liu et al. 2014; Wang et al. 2017; Chen et al. 2019). However, limited studies have been conducted to understand the associations of large-scale climate patterns with the SAT variations over Central Asia (Wang et al. 2008; Chen et al. 2009; Yao et al. 2014). In previous research, a year is commonly divided into four seasons: spring (March-April-May, MAM), summer (June-July-August, JJA), autumn (September-October-November, SON) and winter (December-January-February, DJJ). However, this conventional definition may not be suitable for the Central Asia climate studies because the Central Asia, located in the interior of Eurasia, has a typical continental climate with the characteristics of fairly colder in winter and rather hotter in summer, as well as short durations of spring and autumn. In this study, from the point of monthly average SAT, we firstly define November to March in the next year as the cold season and May to September as the warm season over Central Asia, and then verify the rationality of the definition according to atmospheric circulation evolutions. Next, the dominant modes of the cold season SAT (CSAT) and the warm season SAT (WSAT) over Central Asia are further identified. Finally, we explore the relationships of large-scale climate patterns with the CSAT and the WSAT variations over Central Asia.

2. Data And Methods

Monthly mean surface air temperature used in this study was derived from Climatic Research Unit gridded dataset Version 4.01 (CRU TS4.01) with a horizontal resolution of 0.5°×0.5° (Harris et al. 2014). Large-scale climate indices, including the AO, the East Atlantic/Western Russia (EAWR), the NAO, the Niño 3.4, the Pacific/North American (PNA), the Polar/Eurasia (POL) and the SCAND, were obtained from National Oceanic and Atmospheric Administration (NOAA) Climate Prediction Center (CPC) (https://www.esrl.noaa.gov/psd/data/climateindices/list/). To explain the physical processes associated with the CSAT and the WSAT variations over Central Asia, we also employed monthly atmospheric circulation variables consisting of 500-hPa geopotential height (H500), 850-hPa wind vector (V850) and air temperature at 850-hPa (T850) from ERA5 reanalysis dataset produced by European Centre for Medium-Range Weather Forecasts with a spatial resolution of 0.5°×0.5° (Hersbach et al. 2019). The shortwave radiations, longwave radiations, sensible and latent heat fluxes are obtained from the National Centers for Environment Prediction-US Department of Energy (NCEP-DOE) AMIP-II reanalysis (Kanamitsu et al. 2002). The study period is from January 1979 to December 2016.

We use the EOF analysis (von Storch and Zwiers 1999) to describe the spatial-temporal variation characteristics of the CSAT and the WSAT over Central Asia. The correlation and regression analyses are applied to examine the relationships of the CSAT and the WSAT variations over Central Asia with large-scale climate patterns, and the associated physical mechanisms. We apply Students' *t*-test to assess the statistical significance levels of the correlation and regression analyses.

3. Results

3.1 Definition of the cold season and the warm season over Central Asia

As shown in Fig. 1, the monthly mean SAT values averaged over Central Asia are higher than 15℃ from May to September, and are all below 0℃ for November to March in the next year for the period of 1979–2016. This suggests that we can define the months from November through to the next March as the cold season and the months from May through to September as the warm season over Central Asia. To further justify the suitability of this definition, the time series of winter and summer SAT over Central Asia for the period of 1979–2016 are firstly shown (Fig. 2). The mean SAT values over Central Asia are all less than −4℃ in winter and above 19℃ in summer.

We further analyze and compare the 850hPa wind vector fields in March, April, May, September, October and November with those in winter (December-January-February, DJF) and summer (June-July-August, JJA). Strong southwesterly flows are seen over Central Asia in winter (Fig. 3a), while northwesterly and northeasterly winds are observed in the northern and southern parts, respectively, in summer (Fig. 3b). When considering the wind field in every month other than summer and winter, it reveals that the wind fields in March and November resemble the winter fields (Fig. 3a, c, h), while in May and September, the wind fields is similar with the summer fields (Fig. 3b, d, g). We also calculate the spatial correlation coefficients between the wind directions of 850hPa wind fields in winter with those in every month from January to December over the region extending from 35° to 58°N and from 45° to 90°E. Results indicate that the correlation coefficients in cold months (November-to-March) all exceed 0.60, significant at the 99% confidence level, and they are all small in warm months (May-to-September) (Fig. 4). Combining the results of temperature and wind fields, therefore, the cold season is defined as the months from November to the next March, and the warm season includes the months from May to September over Central Asia.

Based on the new definition, there are altogether 37 cold seasons and 38 warm seasons during the study period of 1979–2016. The cold season of 1979 refers to November 1979 to March 1980, and the 1979 warm season is from May to September in 1979. The dominant modes of the CSAT and the WSAT variations over Central Asia and their linkages with large-scale atmospheric circulation patterns will be discussed in the following sections.

3.2 Dominant modes of the anomalous CSAT and the WSAT variations over Central Asia

We perform the EOF analysis to investigate the temporal and spatial characteristics of the anomalous CSAT and the anomalous WSAT variations with respect to the 1979–2016 climatological values over Central Asia. The first leading EOF mode of the anomalous CSAT over Central Asia (EOF1), explaining 84.5% of the total variance, displays a same-sign structure with the maximum center located over western

Kazakhstan (Fig. 5a). The corresponding EOF1 time series displays a pronounced interannual variability with a period cycle of 2–3 years and weak interdecadal cycle around 10 years (Fig. 5b and Fig. 7a), and is highly related with the regional averaged anomalous CSAT over Central Asia (r = 0.99, the 99.9% confidence level), indicating that the EOF1 of the anomalous CSAT dominates the variation characteristics of the anomalous CSAT over Central Asia.

The second EOF mode (EOF2) of the anomalous CSAT over Central Asia describing 8.7% of the total variance is characterized by a north-south seesaw pattern (Fig. 5c). The corresponding EOF2 time series exhibits an obvious variation (Fig. 5d) with a period cycle of 6–9 years from the power spectrum (Fig. 7b).

The EOF1 mode of the anomalous WSAT over Central Asia features a homogeneous structure, which explains 66.9% of the total variance (Fig. 6a). The corresponding EOF1 time series shows substantial upward trend, and the power spectrum analysis displays a period of 2–3 years cycle variations (Fig. 6b and Fig. 7c). The EOF2 mode of the anomalous WSAT over Central Asia is characterized by a northwest-southeast dipole pattern (Fig. 6c), and the corresponding EOF2 time series displays a high interannual variation with a significant 3-year cycle (Fig. 6d and Fig. 7d). In total, the EOF1 and EOF2 account for more than 81% of the total variance of the anomalous WSAT over Central Asia.

3.3 Large-scale atmospheric circulations related with the CSAT and WSAT anomalies over Central Asia

Figure 8 presents regressions of H500, V850 and T850 onto the EOF1 and EOF2 time series of the anomalous CSAT over Central Asia for the period of 1979–2016. The significantly positive H500 anomalies related with the EOF1 mode of the anomalous CSAT over Central Asia appear over the regions from Central Siberia to Central Asia and Western China while the negative H500 anomalies are observed in Scandinavian Peninsula and eastern Europe in the cold season (Fig. 8a). Correspondingly, an anomalous anticyclonic circulation exists over Central Siberia and surrounding areas, whereas an anomalous cyclonic circulation dominates Scandinavian Peninsula and Eastern Europe (Fig. 8b).

For the EOF2 mode of the anomalous CSAT, the significantly positive H500 anomalies are seen over high-latitude areas, Southern part of Central Asia and many subtropical areas while the significantly negative H500 anomalies mainly appear over Europe and Northwestern Asia (Fig. 8c). For the 850-hPa wind field, the westerly flow is weakened over Northern Central Asia and the southerly flow is slightly enhanced over Southern Central Asia (Fig. 8d).

Figure 9 shows regressions of H500, V850 and T850 onto the EOF1 and EOF2 time series of the anomalous WSAT over Central Asia for the period of 1979–2016. Corresponding to the EOF1 mode of the anomalous WSAT over Central Asia, there are strong positive H500 anomalies over the region extending from Eastern Europe to Central Asia, accompanied by an anomalous anticyclonic circulation in the 850-hPa wind field in the warm season (Fig. 9a, b). For the EOF2, significantly negative H500 anomalies are observed over the region from Eastern Europe to Northwestern Central Asia with an anomalous cyclone in

the 850-hPa wind field (Fig. 9c, d). Regardless of the cold season or the warm season, the positive H500 anomalies can provide favorable conditions for the warm SAT anomalies over Central Asia and other regions maybe via the enhancements of solar radiation reaching land surface and subsidence warming.

To investigate how the warm CSAT and WSAT anomalies over Central Asia are induced, we examined the effects of surface heat flux and advection. Figures 10 and 11 show the CSAT-related and WSAT-related anomalies surface net radiation (NR), sensible heat flux (SHF), net shortwave radiation (SWR),and net longwave radiation (LWR) from1979 to 2016. Positive NR represents downward direction, which is favor of heating surface. Corresponding to the EOF1 of the anomalous CSAT, positive NR is observed throughout most Central Asia (Fig. 10a), which is dominated by downward SWR (Fig. 10b). This is likely attributed to the clear sky accompanied by the anomalous anticyclone (Fig. 8a). Although the LWR tends to cool the ground (Fig. 10c), its effect is weaker than the SWR (Fig. 10b and 10c). These results indicate that the ground surface receives more heat from the downward solar radiation to warm the surface (Fig. 10a).When the ground is heated and warmer than the surface air, it will lead to upward sensible heat flux to warm the air (Fig. 10b), thereby contributing constructively to the warmer CSAT (Fig. 8b).

For the EOF2 of the anomalous CSAT, negative CSAT anomalies over Northeastern parts of Central Asia are attributed to significant negative NR anomalies dominated by the cooling effect of upward LWR (Fig. 8d, 10f, 10h), while weaker positive NR anomalies exist in Middle parts of Central Asia, which are contributed to the formation of positive CSAT anomalies in these regions (Fig. 8d, 10f). However, the spatial distribution of the NR anomalies (Fig. 10f) are different from that of the CSAT anomalies to some extent (Fig. 8d). Positive CSAT anomalies over Western parts of Central Asia cannot be explained by NR increase.

Corresponding to the EOF1 of the anomalous WSAT, significant positive NR anomalies are seen around Western and Northern parts of Central Asia where positive WSAT anomalies center are observed (Fig. 11a, 7b), which is mainly due to downward SWR increase (Fig. 11b) brought by positive H500 and anomalous anticyclone at V850 (Fig. 9a, 9b). The WSAT over Eastern Central Asia is also a positive anomaly (Fig. 9b), nevertheless there are controlled by negative NR anomalies due to upward SWR and LWR increase (Fig. 11a-c). These indicate that the formation of the EOF1 of anomalous WSAT over Central Asia can be partly explained by the NR anomalies.

Corresponding to the EOF2 of the anomalous WSAT, the spatial distribution of NR anomalies (Fig. 10f) are similar with that of the anomalous WSAT, showing a northwest-southeast dipole distribution (Fig. 6c, 9d, 11f). Negative WSAT anomalies corresponds to negative NR anomalies over Northwestern of Central Asia, while the opposite phenomenon is in Southeastern Central Asia. Above analysis indicates that surface heat flux changes over many regions of Central Asia can explain the formation of CSAT and WSAT anomalies associated with the first two EOF modes.

A further inspection suggests that the advection of basic temperature by anomalous winds is constructive (Fig. 12c), while the advection of anomalous temperature by basic wind is destructive (Fig. 12b) for the EOF1 of anomalous CSAT (Fig. 8b). To better understand this process, we also shows

the climatological mean winds overlaid on the EOF1of anomalous CSAT-related temperature anomalies (Fig. 14a) and the EOF1 of anomalous CSAT-related wind anomalies overlaid on the climatological mean temperature (Fig. 14b). Results show that the anomalous wind can advect the warm air northeastward towards the Central Asia, leading to warming tendency over Central Asia (Fig. 12c, 14b, 8b).

For the EOF2 of anomalous CSAT, the CSAT-related warm center is right located to the southwestern of Central Asia; therefore, the warm air advection flow northeastward towards the Central Asia by the climatological mean wind (Fig. 14c); what's more, the anomalous wind can also advect the warm air from low latitudes to Southern of Central Asia (Fig. 12e). These contribute to warming tendency CSAT anomalies over Southern part of Central Asia (Fig. 8d). Although the CSAT anomalies over the Northern part of Central Asia is affected by the warm advection brought by the climatological wind (Fig. 12d, 12e, 14c), but also due to the cancellation of the cold advection brought by the anomalous wind (Fig. 12f, 14d), causing the CSAT variations over Northern part of Central Asia is weak, even in the Northeast Central Asia, the CSAT is negative anomalies (Fig. 8d).

For the EOF1 of the anomalous WSAT over Central Asia, the climatological wind tends to warm WSAT over Central Asia due to due to the advection of warm air from the anomalous warm center located in Northwest Central Asia flow eastward and southward towards Central Asia (Fig. 9b, 15a). In contrast, the anomalous anticyclone (Fig. 9b) favors cooling tendency over Central Asia (Fig. 9b) because the climatological wind blow up-gradient of the anomalous temperature field (Fig. 15b). Despite this seemingly destructive effect, this anomalous anticyclone is crucial for the formation of the anomalous warm center over Northeast of Central Asia (Figs. 9b and 15a) because the southerly wind anomalies of the anticyclone blows down-gradient of the climatological mean temperature field (Fig. 15b).

Corresponding to the EOF2 of WSAT over Central Asia, the WSAT-related cold center is right located to the Northwest of Central Asia (Fig. 15c); the cold air advection accompanied by the climatological northwesterly wind therefore lead to negative WSAT anomalies over Northwest portion of Central Asia (Fig. 9d, 15c). However, the warm WSAT anomalies over Eastern and Southern of Central Asia (Fig. 9d) is partly attributed to the warm air advection brought by the southwesterly wind in the south of anomalous cyclone (Fig. 15d).

3.4 Linkages of large-scale climate patterns with the CSAT and WSAT variations over Central Asia

Previous studies suggest that the large-scale atmospheric circulation changes may play an important role in the SAT anomalies over Central Asia (Wang and Wei, 2012; Zhou et al., 2016; Luo et al., 2019). In the analysis that follows, we further investigate the large-scale climate patterns anomalies association with the first two EOF modes of Central Asia CSAT and WSAT variations. Results show that the EOF1 time series of the anomalous CSAT over Central Asia is closely related with the SCAND in the cold season with correlation coefficient of -0.63 for 1979–2016, significant at the 99% confidence level. Meanwhile, the EOF2 time series of the anomalous CSAT over Central Asia is highly correlated with the AO and the NAO in the cold season. Compared with the AO, correlation with the NAO is much weaker (Fig. 16a). These

results suggest that the SCAND and the NAO have substantial roles to play in influencing the CSAT variation over Central Asia. Correlations between the other large-scale climate indices shown in Fig. 16a and the first two EOF time series of the anomalous CSAT over Central Asia are not significant.

The EOF1 time series of the anomalous WSAT over Central Asia is tightly associated with the EAWR and the NAO in the warm season. Among them, the correlation coefficient with the EAWR index is the strongest, reaching up to -0.58, followed by the NAO index with correlation coefficient of -0.53 (Fig. 16b). These correlations are all significant at the 99% confidence level based on Student's *t*-test. The EOF2 time series of the WSAT over Central Asia is significantly correlated with the EAWR index ($r = 0.36$, the 95% confidence level). These indicate that the atmospheric circulation anomalies related with EAWR and NAO play an important role in modulating the WSAT anomalies over Central Asia.

We further examine the relationships of the SCAND and the AO to the CSAT variations over Central Asia for the period of 1979–2016 (Fig. 17). The positive phase of the SCAND tends to correspond to significantly negative CSAT anomalies over Central Asia in the cold season (Fig. 17a), whereas the AO show a north-south dipole pattern, roughly similar to the EOF2 mode of the CSAT over Central (Fig. 17b and 4c) Asia with significantly positive correlations center of CSAT anomalies appearing over Northeastern areas of Central Asia (Fig. 17b).

In the warm season, the anomalous WSAT over Central Asia is negatively correlated with the EAWR and the NAO for 1979–2016 (Fig. 10). Significant correlations appear over almost the whole Central Asia both these two climate patterns (Fig. 18a and b), the maximum correlation coefficient center mainly show over Western and Central parts of Central Asia for the EAWR and the NAO (Fig. 18a 18b) .

To further confirm roles of the SCAND and the AO patterns in the variation of anomalous CSAT over Central Asia, we display H500 and V850 wind anomalies by regression onto the SCAND and the AO indices, as shown in Fig. 19. During negative phase of the SCAND pattern, the Central Asia is dominated by significant negative H500 anomaly in the cold season with the center existing in the Lake Baikal (Fig. 19c), accompanying cold advection from Siberia to Central Asia led to the negative CSAT anomalies over Central Asia, especially in Northeastern parts of Central Asia (Fig. 19d, 9b and 15b). For the large-scale atmospheric circulation associated with the AO pattern, the positive CSAT anomalies over the Northeastern of Central Asia is affected by the significant southwesterly winds; while the negative CSAT anomalies over Southwestern parts of Central Asia is attributed to anomalous significant northwesterly winds associated with the anticyclonic circulation in Western Europe (Fig. 19a, b and 9b, c).

In the warm season, the significant negative H500 anomaly associated with the positive EAWR pattern occupy the most areas of Central Asia with the notable negative center located in Northwestern of Central Asia (Fig. 20c). Therefore, the cooling of the WSAT in the Northwestern Central Asia is more significantly due to the significant northwesterly wind on the north of the cyclone conveying cold and dry air flow from high latitude (Fig. 20d and 18a). However, the remarkable negative H500 anomaly center related with NAO pattern is located in Central Asia (Fig. 20a), which has an impact on the WSAT all the whole region of Central Asia (Fig. 20b and 18b).

4. Conclusions

Central Asia is characterized by a remarkable continental climate, and has short durations of spring and autumn. Based on the analyses of monthly mean SAT and atmospheric circulation, we define the months from November through to the next March as the cold season and May to September as the warm season, and further investigate dominant modes of the CSAT and WSAT variations over Central Asia connected with large-scale climate patterns for the period of 1979–2016.

The EOF analysis shows that the first leading mode of the CSAT variation over Central Asia, describing 84.5% of the total variance, is featured by a monopole pattern with the maximum center appearing over western Kazakhstan. The EOF2 mode of the CSAT over Central Asia is characterized by a south-north dipole pattern. The EOF1 and EOF2 modes of the WSAT over Central Asia mainly show homogeneous and northwest-southeast variations, describing 66.9% and 14.4% explanatory variances, respectively. The EOF1 and EOF2 together account for about 93% and above 81% of the total variances for the CSAT and the WSAT variations, respectively.

The atmospheric circulation patterns play a crucial role in driving the CSAT and the WSAT variations over Central Asia. For the EOF1 mode of the CSAT over Central Asia, warm anomalies correspond to a significant positive H500 anomaly and anomalous southwesterly winds at V850 over Central Asia. These subsequently maybe heat the CSAT over Central Asia by enhancing the downward solar radiation, strengthening the subsidence warming and warm advection. For the EOF2 mode of the CSAT over Central Asia, positive CSAT anomaly over the southwestern Central Asia is related with the significant southwesterly winds carrying warm air from low latitudes, while negative CSAT anomaly is attributed to the significant northeasterly winds which bring cold air to the northeastern Central Asia from high latitudes.

The large-scale atmospheric circulations associated with the EOF1 of the WSAT over Central Asia show that the anomalous notable positive H500 dominants over Central Asia, generally contributed to positive WSAT anomaly via subsidence warming. Corresponding the EOF2 of the WSAT over Central Asia, the wind-induced play an important impact on the WSAT anomaly. The anomalous southwesterly wind at V850 are in favor of the positive WSAT anomaly over the southeastern Central Asia. By contrast, the negative WSAT anomaly over the northwestern Central Asia cause by the anomalous northwesterly wind.

Combining the EOF and correlation analyses, the SCAND and the AO are identified to be closely related with the SAT variations over Central Asia in the cold season, while the EAWR and the NAO are supposed to influence the WSAT variations over Central Asia to varying degrees. For example, the negative phase of the SCAND tends to result in strongly warm anomalies over the whole Central Asia while the EAWR may mainly play a substantial role over Western part in the warm season. Further analysis indicates that these large-scale climate patterns tend to cause the CSAT and WSAT anomalies over Central Asia via their effects on regional geopotential heights, wind-induced warm advections and other processes.

This study analyzes dominant modes of the CSAT and WSAT variations over Central Asia and their close linkages to large-scale climate patterns, and may help to improve the SAT predictions over this region. Meanwhile, other driving factors such as land surface conditions should be further explored (Zhang et al., 2011; Wei and Dirmeyer, 2012), and understanding thermodynamic and dynamic processes influencing the SAT variations in the cold and warm season needs to be deepened in the future.

Declarations

Acknowledgments

We thank the three anonymous reviewers for their constructive comments that help to improve the quality of the manuscript.

Conflict of Interest

All the authors have no conflicts of interest to declare.

Funding Statement

This work was supported by the National Key Research and Development Program of China (2018YFA0606501) and the National Natural Science Foundation of China (Grant No. 41675085).

Authors' Contributions

Yuanhuang Zhuang downloaded and analyzed all the data in this study and was a major contributor in writing the manuscript.

Jingyong Zhang conceived the whole framework of the article. All the authors have modified the content and format of the paper.

All authors read and approved the final manuscript.

Availability of data and material

The CRU TS4.01 data is available at https://crudata.uea.ac.uk/cru/data/hrg/. The large-scale atmospheric indices are stored at https://www.esrl.noaa.gov/psd/data/climateindices/list/. The monthly ERA-5 reanalysis atmospheric circulation variables of 500-hPa geopotential height, 850-hPa wind vector and air temperature at 850-hPa are available at https://cds.climate.copernicus.eu/cdsapp#!/dataset/reanalysis-era5-pressure-levels-monthly-means?tab=form. The NCEP-DOE AMIP-II reanalysis data is available at https://psl.noaa.gov/data/gridded/data.ncep.reanalysis2.gaussian.html.

Code availability

The code that supports the findings of this study is not available

Ethics Approval

Not applicable

Consent to participate

Not applicable

Consent for publication

Not applicable

References

1. Barnston AG, Livezey RE (1987) Classification, seasonality and persistence of low frequency atmospheric circulation patterns. Mon Wea Rev 115(6):1083–1126
2. Besselaar EJMVD, Tank AMGK, Schrier GVD (2010) Influence of circulation types on temperature extremes in Europe. Theor Appl Climatol 99(3):431–439
3. Chen F, An C, Dong G, Zhang D (2017) Human activities, environmental changes, and rise and decline of Silk Road civilization in Pan-Third Pole region. Bulletin of Chinese Academy of Sciences (in Chinese) 32(9):967–975
4. Chen F, Wang J, Jin L, Zhang Q (2009) Rapid warming in mid-latitude central Asia for the past 100 years. Frontiers of Earth Science 3(1):42–50
5. Chen S, Wu R, Song L, Chen W (2018) Combined influence of the Arctic Oscillation and the Scandinavia pattern on spring surface air temperature variations over Eurasia. Journal of Geophysical Research: Atmospheres 123(17):9410–9429
6. Chen S, Wu R, Song L, Chen W (2019) Interannual variability of surface air temperature over mid-high latitudes of Eurasia during boreal autumn. Clim Dyn 53:1805–1821
7. Gong D, Wang S, Zhu J (2001) East Asian winter monsoon and Arctic oscillation. Geophys Res Lett 28(10):2073–2076
8. Guo YP, Li JP (2016) Impact of ENSO events on the interannual variability of Hadley circulation extents in boreal winter. Advances in Climate Change Research 7(1):46–53
9. Harris I, Jones PD, Osborn TJ, Lister DH (2014) Updated high-resolution grids of monthly climatic observations - the CRU TS3.10 Dataset. Int J Climatol 34(3):623–642
10. Hersbach H, Bell W, Berrisford P, Horányi AJM-S, Nicolas J, Radu R, Schepers D, Simmons A, Soci C, Dee D (2019) Global reanalysis: Goodbye ERA-Interim, hello ERA5. ECMWF Newsletter 159:17–24
11. Hoy A, Sepp M, Matschullat J (2013) Large-scale atmospheric circulation forms and their impact on air temperature in Europe and northern Asia. Theor Appl Climatol 113(3):643–658
12. Hurrell JW, Loon HV (1997) Decadal variations in climate associated with the Northampton oscillation. Clim Change 36:301–326

13. Hu Z, Zhang C, Hu Q, Tian H (2014) Temperature Changes in Central Asia from 1979 to 2011 Based on Multiple Datasets. J Clim 27(3):1143–1167
14. Hu Z, Zhou Q, Chen X, Qian C, Wang S, Li J (2017) Variations and changes of annual precipitation in Central Asia over the last century. Int J Climatol 37(Suppl. 1):157–170
15. Huang JP, Li Y, Fu C, Chen F, Fu Q, Dai A, Shinoda M, Ma Z, Guo W, Li Z, Zhang L, Liu Y, Yu H, He Y, Xie Y, Guan X, Ji M, Lin L, Wang S, Yan H, Wang G (2017) Dryland climate change: Recent progress and challenges. Rev Geophys 55(3):719–778
16. IPCC (2013) Summary for policymakers. Fifth Assessment Report of the Intergovernmental Panel on Climate Change. Cambridge University Press, Cambridge
17. Koide H, Kodera K (1999) A SVD analysis between the winter NH 500-hPa height and surface temperature fields. J Meteorol Soc Jpn 77(1):47–61
18. Li JP, Wang JXL (2003) A new North Atlantic Oscillation index and its variability. Adv Atmos Sci 20(5):661–676
19. Lioubimtseva E, Cole R, Adams JM, Kapustin G (2005) Impacts of climate and land-cover changes in arid lands of Central Asia. J Arid Environ 62(2):285–308
20. Lioubimtseva E, Henebry CM (2009) Climate and environmental change in arid Central Asia: Impacts, vulnerability, and adaptations. J Arid Environ 73(11):963–977
21. Liu YY, Wang L, Zhou W, Chen W (2014) Three Eurasian teleconnection patterns: Spatial structures, temporal variability, and associated winter climate anomalies. Clim Dyn 42(11):2817–2839
22. Luo M, Liu T, Meng F, Duan Y, Bao A, Frankl A, Maeyer PD (2019) Spatiotemporal characteristics of future changes in precipitation and temperature in Central Asia. Int J Climatol 39(3):1571–1588
23. Ren H, Zuo J, Jin FF, Stuecker MF (2015) ENSO and annual cycle interaction: the combination mode representation in CMIP5 models. Clim Dyn 46(11):3753–3765
24. Santoso A, Mcphaden MJ, Cai W (2017) The defining characteristics of ENSO extremes and the strong 2015/16 El Niño: ENSO extremes. Rev Geophys 55(4):1079–1129
25. Steinbrecht W, Claude H, Köhler U, Winkler P (2001) Interannual changes of total ozone and Northern Hemisphere circulation patterns. Geophys Res Lett 28(7):1191–1194
26. Thompson DWJ, Wallace JM (1998) The Arctic oscillation signature in the wintertime geopotential height and temperature fields. Geophys Res Lett 25(9):1297–1300
27. Thompson DWJ, Wallace JM (2000) Annular modes in the extratropical circulation-Part I Month-to-month variability. J Clim 13(5):1000–1016
28. Victoria VC, Jones PD, Davies TD (2001) Atmospheric circulation and surface temperature in Europe from the 18th century to 1995. Int J Climatol 21(1):63–75
29. Von Storch H, Zwiers FW (1999) Statistical analysis in climate research. Cambridge Univ Press, Cambridge, pp 293–299
30. Wang J, Chen F, Jin L, Guo J (2008) Relationships between climatic anomaly in arid region of centre-east Asia and sea level pressure anomaly in the last 100 years. Plateau Meteorology (in Chinese)

27(1):84–95

31. Wang JS, Wei F (2012) Impact of 500hpa height field anomaly on precipitation and temperature change over arid Central Asia over the past 100 years. In: 2012 IEEE International Geoscience and Remote Sensing Symposium. 22–27 July 2011. Munich, Germany, 868–871
32. Wang C, Bo Y, Li R, Bo H (2016) Impacts of the Asia–Australia dipole and ENSO on climate variability in the Asia–Australia region. Int J Climatol 36(13):4202–4212
33. Wang X, Li J, Sun C, Liu T (2017) NAO and its relationship with the Northern Hemisphere mean surface temperature in CMIP5 simulations. Journal of Geophysical Research: Atmospheres 122(8):4202–4227
34. Wei J, Dirmeyer PA (2012) Dissecting soil moisture-precipitation coupling. Geophys Res Lett 39(19):L19711
35. Wu B, Wang J (2002) Winter arctic oscillation, Siberian high and East Asian winter monsoon. Geophys Res Lett 29(19):1–4
36. Wu R, Yang S, Liu S, Sun L, Lian Y, Gao Z (2010) Changes in the relationship between northeast China summer temperature and ENSO. Journal of Geophysical Research: Atmospheres 115(D21):D21107
37. Wu ZW, Wang B, Li J, Jin FF (2009) An empirical seasonal prediction model of the East Asian summer monsoon using ENSO and NAO. Journal of Geophysical Research: Atmospheres 114(D18):D18120
38. Yang S, Lau KM (1998) Influences of sea surface temperature and ground wetness on Asian summer monsoon. J Clim 11(12):3230–3246
39. Yao JQ, Liu ZH, Yang Q, Liu Y, Li CZ, Hu WF (2014) Temperature variability and its possible causes in the typical basins of the arid Central Asia in recent 130 years. Acta Geographica Sinca (in Chinese) 69(3):291–302
40. Zhai P, Yu R, Guo Y, Li Q, Ren X, Wang Y, Xu W, Liu Y, Ding Y (2016) The strong El Niño in 2015/2016 and its dominant impact on global and China's climate. J Meteor Res 74(3):283–297
41. Zhang J, Wu L, Huang G, Zhu W, Yang Z (2011) The role of May vegetation greenness on the southeastern Tibetan Plateau for East Asian summer monsoon prediction. Journal of Geophysical Research: Atmospheres 116(D05):D05106
42. Zhang J, Zhuang Y, Li C, Wang Y, Gu B, Tan X (2018) Temporal and spatial analyses of climate change and extreme events over major areas of the Belt and Road. China Meteorological Press (in Chinese) Beijing
43. Zhang W, Li H, Stuecker MF, Jin FF, Turner AG (2016) A New Understanding of El Niño's Impact over East Asia. J Clim 29(12):4347–4359
44. Zhu X, Wei Z, Dong W, Ji Z, Wen X, Zheng Z, Yan D, Chen D (2020) Dynamical downscaling simulation and projection for mean and extreme temperature and precipitation over central Asia. Clim Dyn 54:3279–3306

45. Zhuang Y, Zhang J, Wang L (2018) Variability of cold season surface air temperature over northeastern China and its linkage with large-scale atmospheric circulations. Theor Appl Climatol 132(3):1261–1273
46. Zhou Y, Lu Y, Yang B, Jiang J, Huang A, Zhao Y, La M, Yang Q (2016) On the relationship between the Maddenmgulian Oscillation and 2m air temperature over central Asia in boreal winter. Journal of Geophysical Research Atmospheres 121(22):13250–13272

Figures

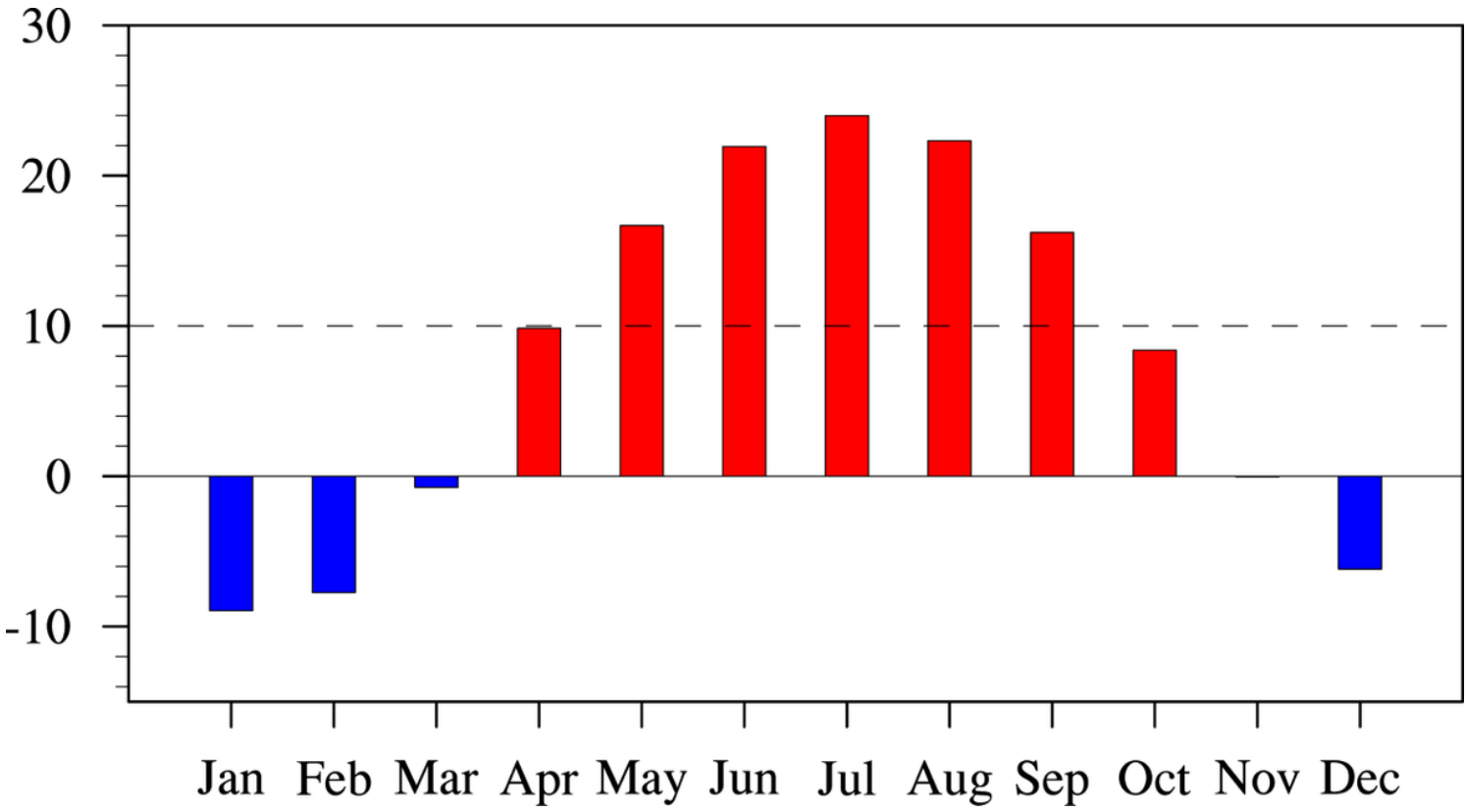

Figure 1

The monthly mean surface air temperature (SAT) averaged over Central Asia from January to December for the period of 1979–2016 (unit: °C; the black dashed line indicates 10°C; Central Asia includes Kazakhstan, Uzbekistan, Turkmenistan, Tajikistan and Kyrgyzstan in this study).

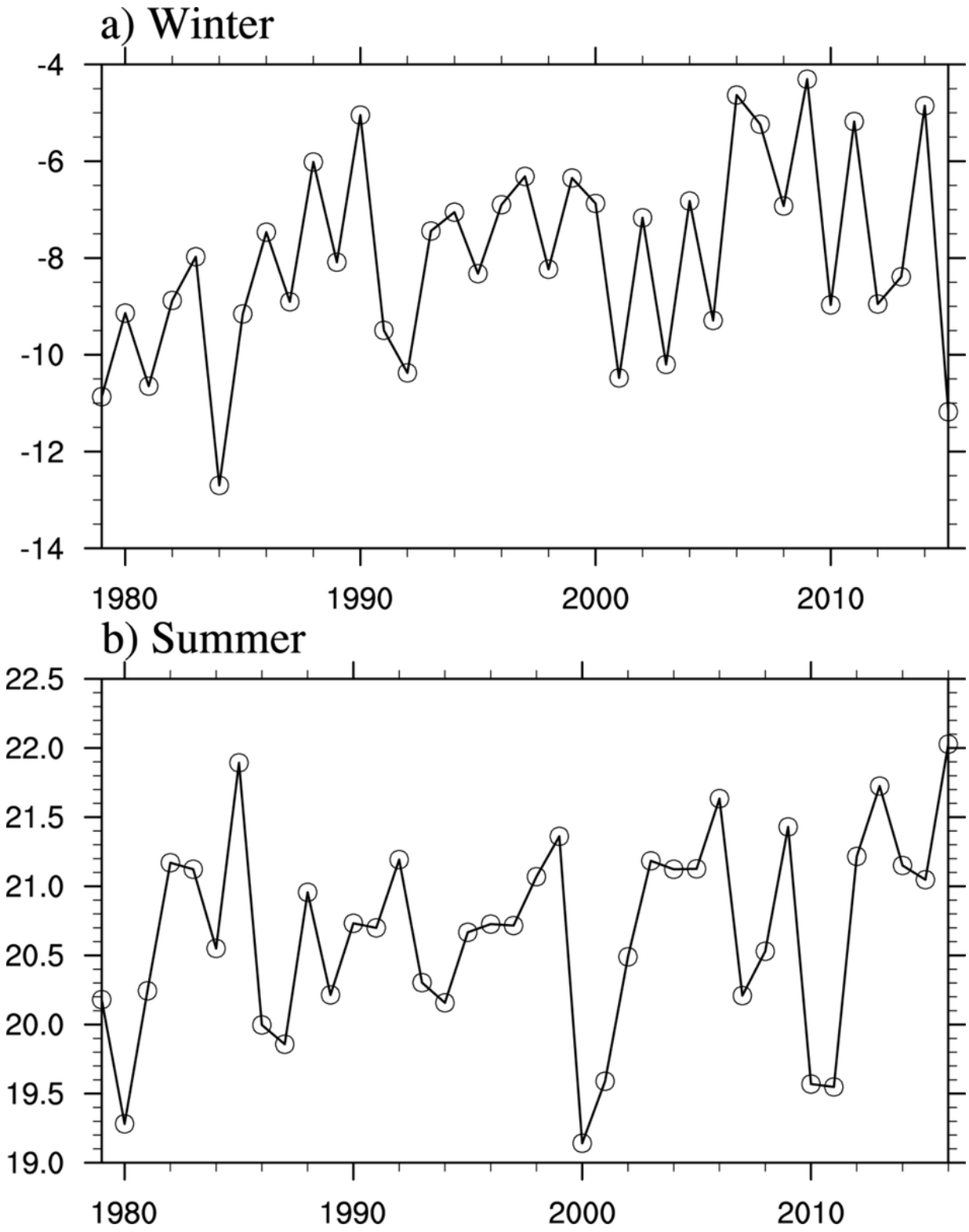

Figure 2

The time series of a winter (December-January-February, DJF) and b summer (June-July-August, JJA) SAT over Central Asia for the period of 1979-2016.

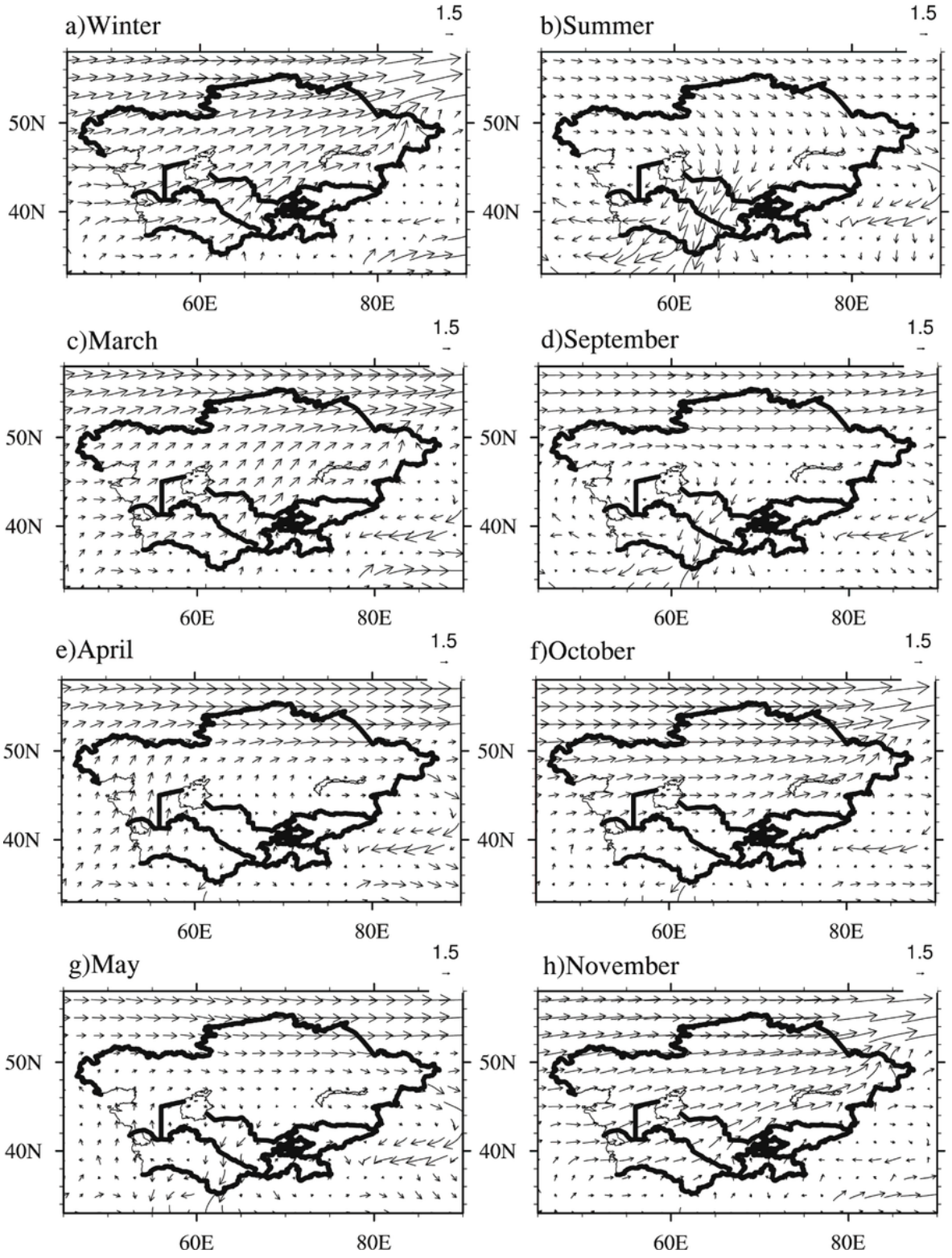

Figure 3

The climatological 850-hPa wind fields during the period of 1979–2016 for a Winter (December-January-February, DJF), b Summer (June-July-August, JJA), c March, d September, e April, f October, g May, h November (m·s-1; vectors; scale at upper-right corner). Note: The designations employed and the presentation of the material on this map do not imply the expression of any opinion whatsoever on the part of Research Square concerning the legal status of any country, territory, city or area or of its

authorities, or concerning the delimitation of its frontiers or boundaries. This map has been provided by the authors.

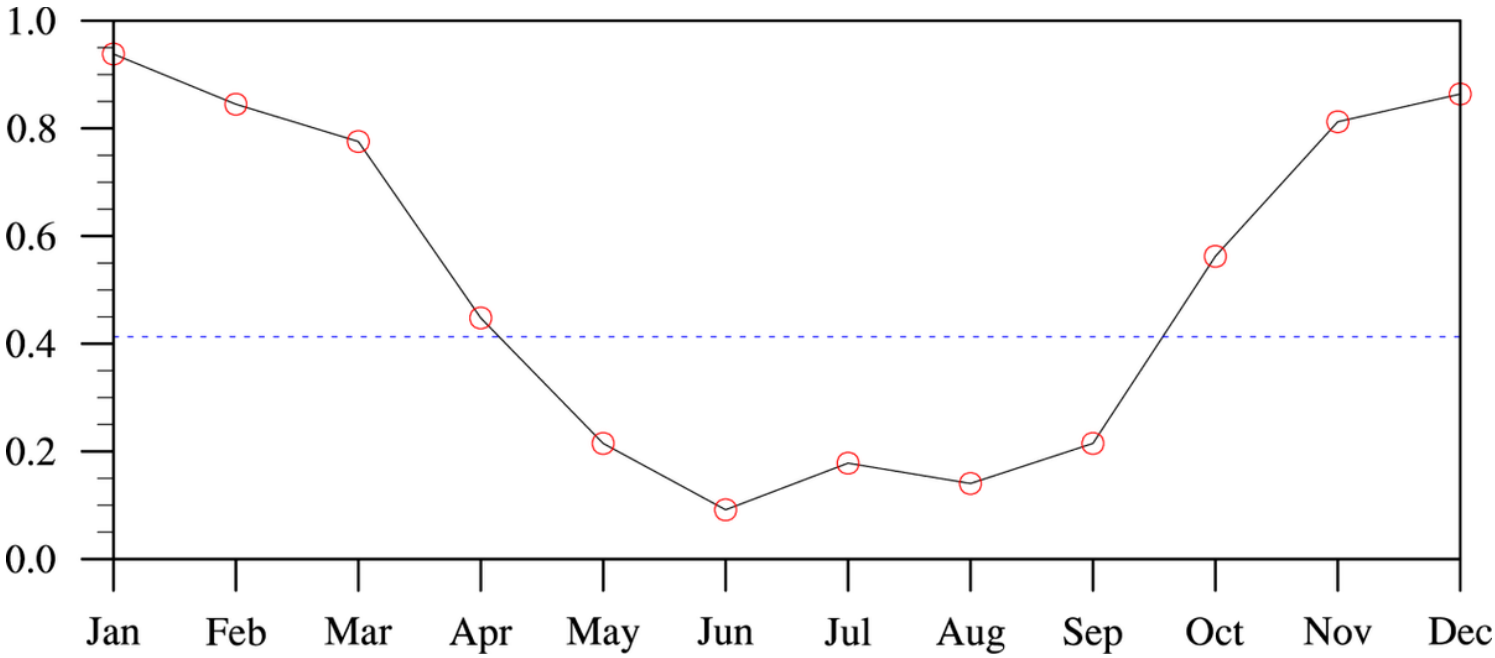

Figure 4

Correlation coefficients of the wind directions between the winter and the months from January to December at 850-hPa over the regions extending from 35° to 58°N and from 45° to 90°E for the period of 1979-2016 (The blue dashed line denotes the 99% confidence level based on a two-sided Student's t-test).

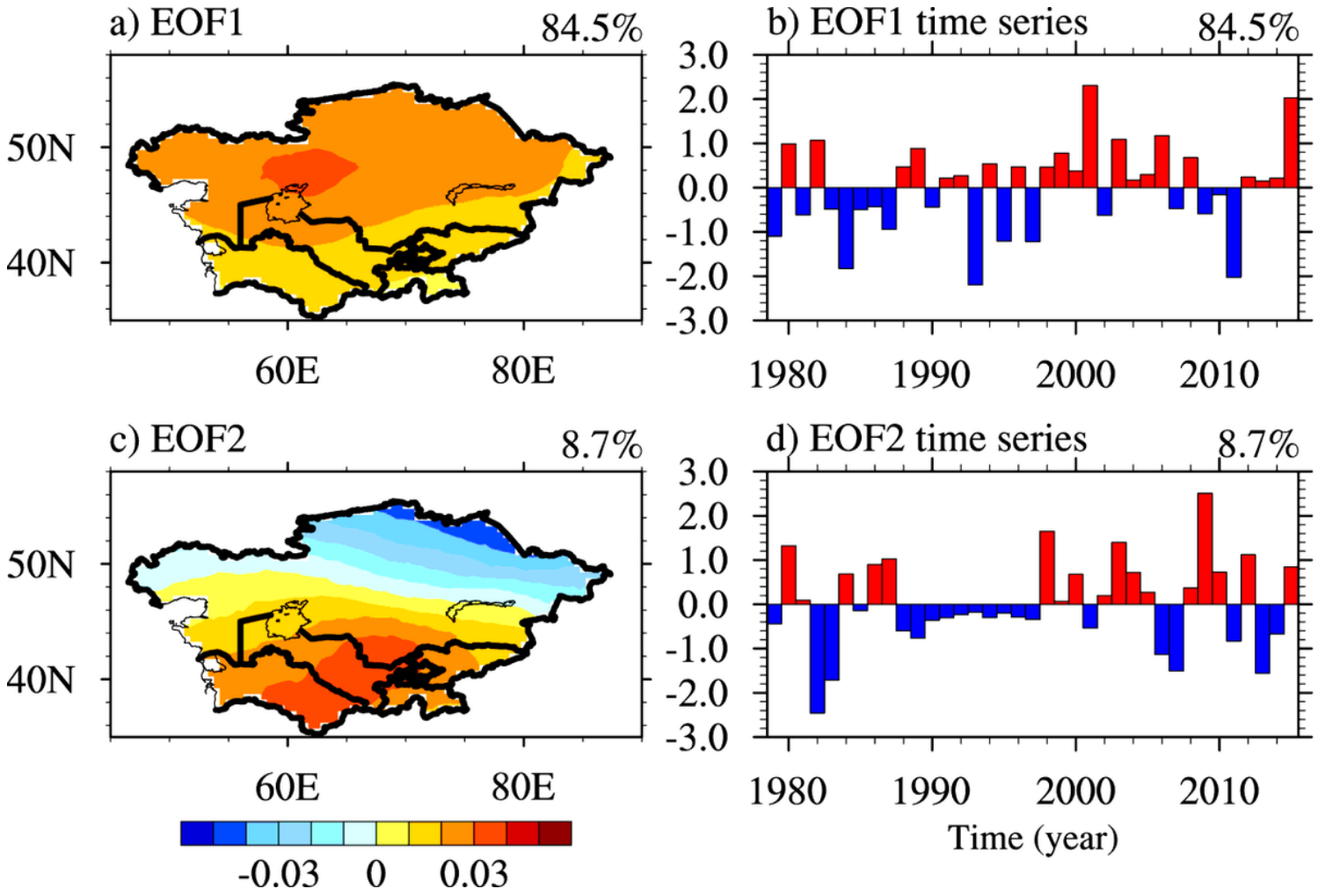

Figure 5

Spatial distributions of the first two EOF modes of the anomalous CSAT over Central Asia and the corresponding normalized time series for the period of 1979-2016: a EOF1, b EOF1 time series, c EOF2, d EOF2 time series. Note: The designations employed and the presentation of the material on this map do not imply the expression of any opinion whatsoever on the part of Research Square concerning the legal status of any country, territory, city or area or of its authorities, or concerning the delimitation of its frontiers or boundaries. This map has been provided by the authors.

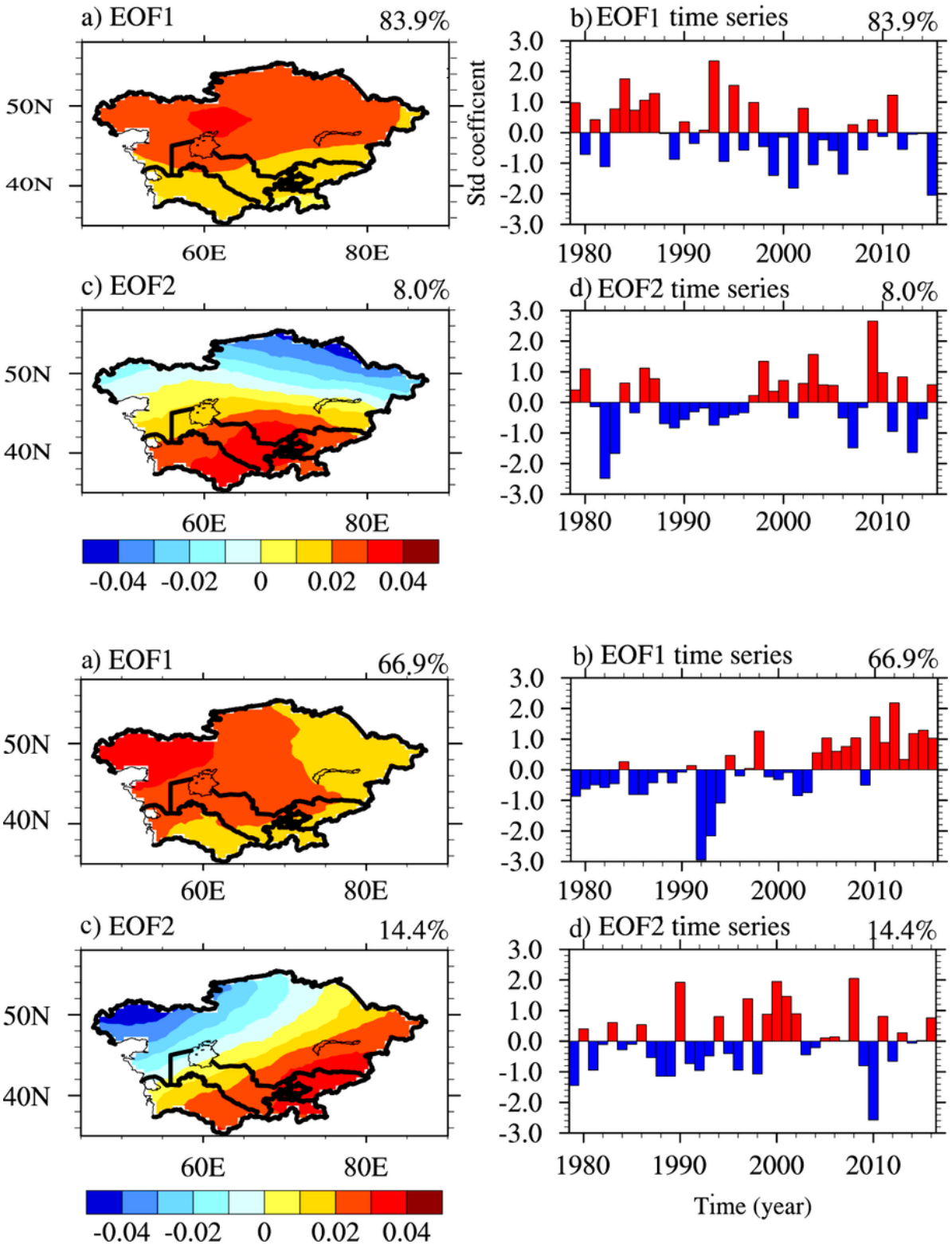

Figure 6

Same as Fig. 5, but for the anomalous WSAT over Central Asia. Note: The designations employed and the presentation of the material on this map do not imply the expression of any opinion whatsoever on the part of Research Square concerning the legal status of any country, territory, city or area or of its authorities, or concerning the delimitation of its frontiers or boundaries. This map has been provided by the authors.

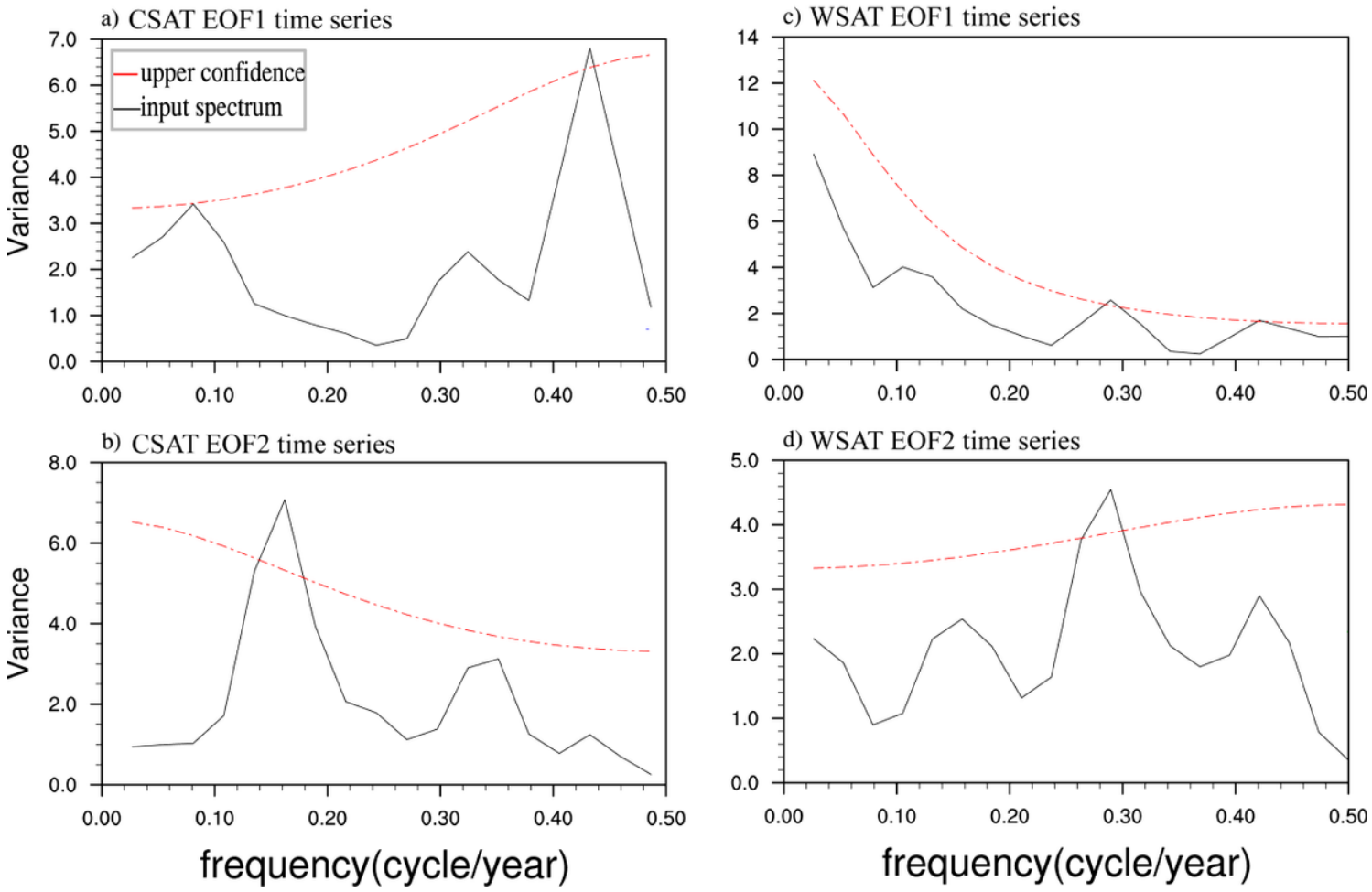

Figure 7

Power spectrums of the corresponding normalized first two EOF time series of the anomalous CSAT and WSAT over Central Asia for the period of 1979-2016: a, b EOF1 time series, c, d EOF2 time series.

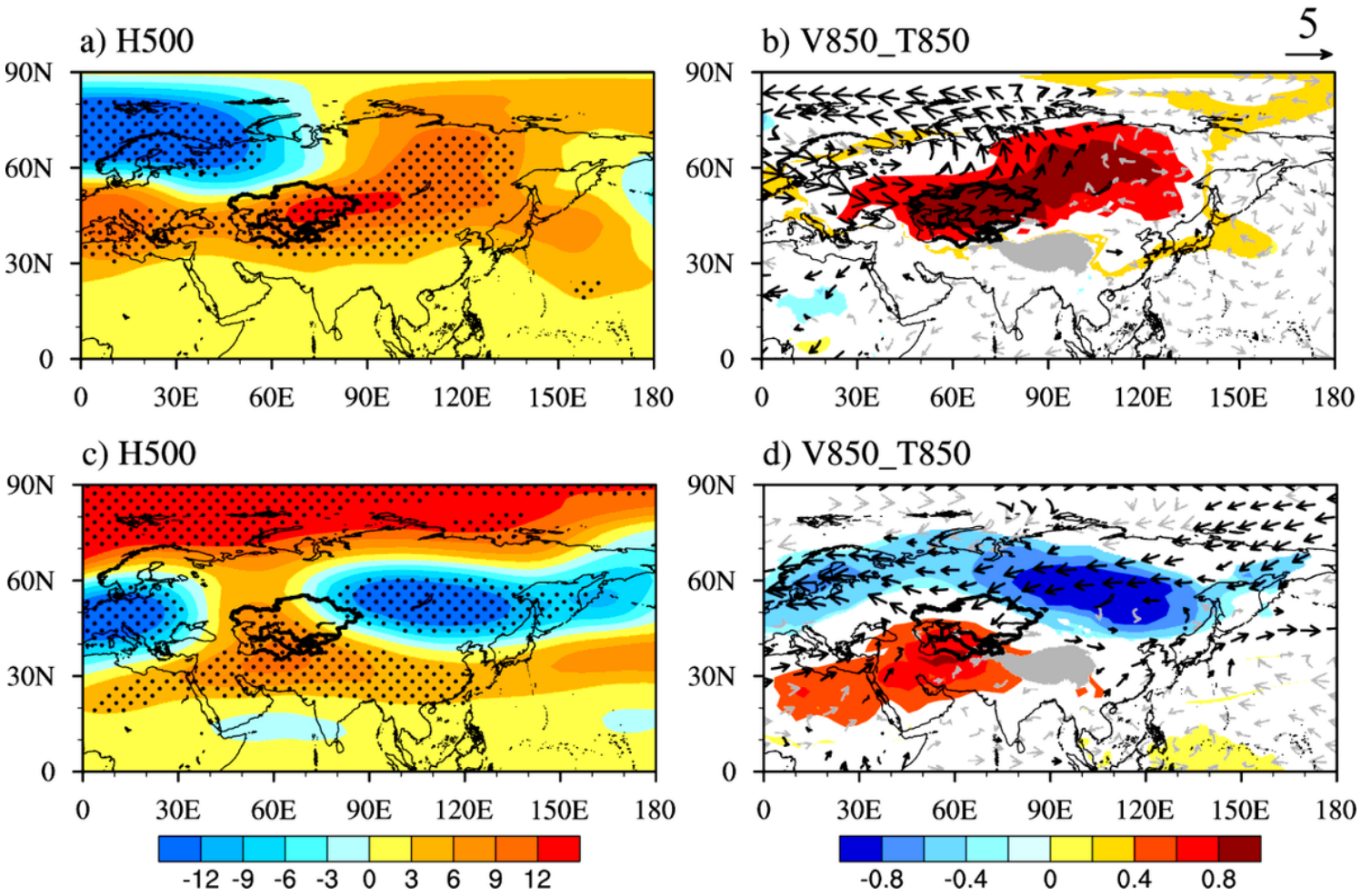

Figure 8

Regression maps of H500, V850 and T850 associated with the EOF1 and EOF2 time series of the anomalous CSAT over Central Asia for the period of 1979-2016: a, b the EOF1; c, d the EOF2; H500, V850 and T850 denote 500-hPa geopotential height, 850-hPa wind vector, and 850-hPa air temperature, respectively. (The black dot in a and c, the color shadows and black arrows in b and d indicates the 95% confidence levels based on a two-sided Student's t-test. The contour intervals of H500, V850 and T850 are 3gpm, 5m·s-1 and 0.2°C respectively. The Central Asia is marked by the black lines). Note: The designations employed and the presentation of the material on this map do not imply the expression of any opinion whatsoever on the part of Research Square concerning the legal status of any country, territory, city or area or of its authorities, or concerning the delimitation of its frontiers or boundaries. This map has been provided by the authors.

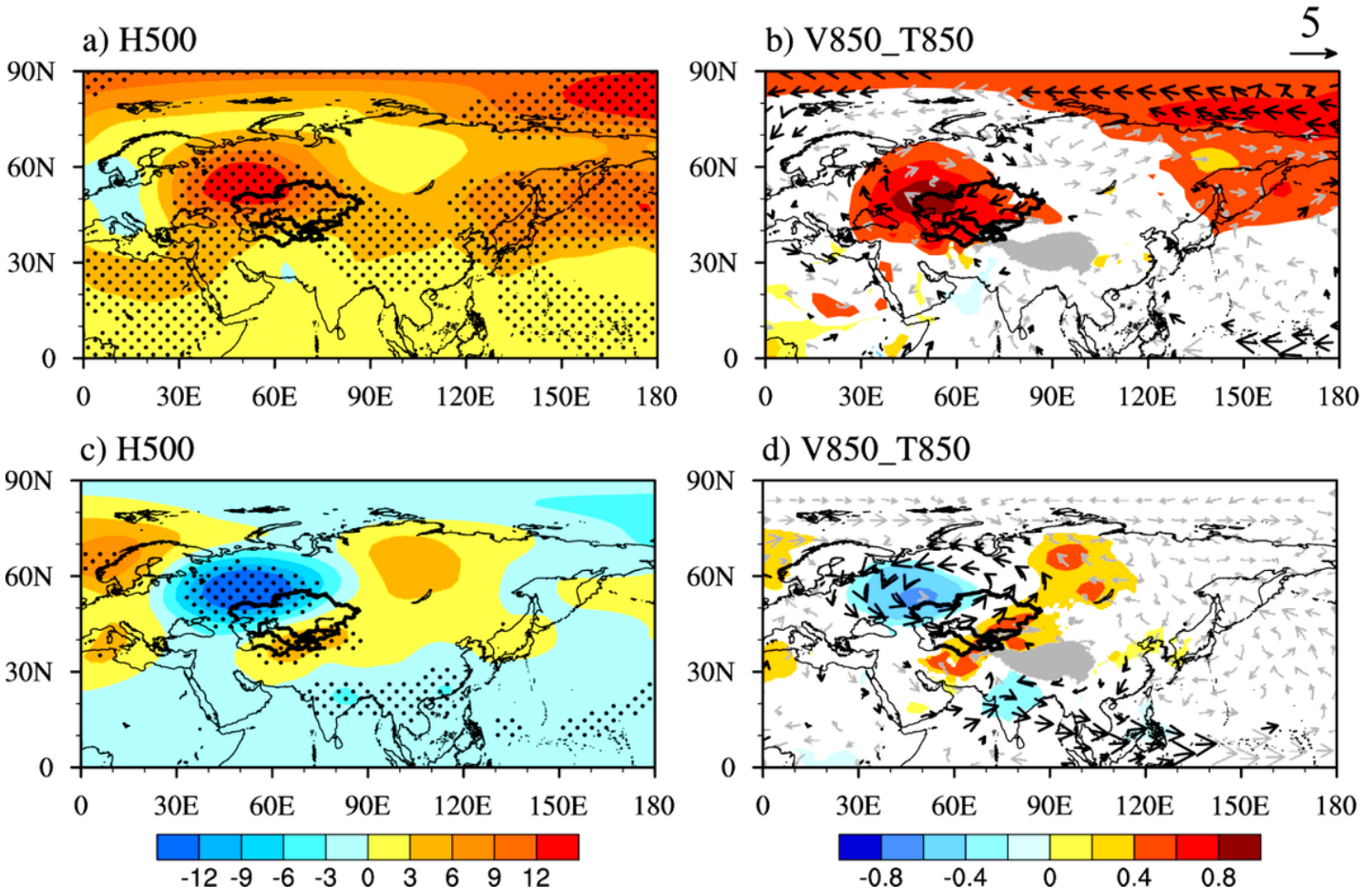

Figure 9

Same as Fig. 10, but for the anomalous WSAT over Central Asia. Note: The designations employed and the presentation of the material on this map do not imply the expression of any opinion whatsoever on the part of Research Square concerning the legal status of any country, territory, city or area or of its authorities, or concerning the delimitation of its frontiers or boundaries. This map has been provided by the authors.

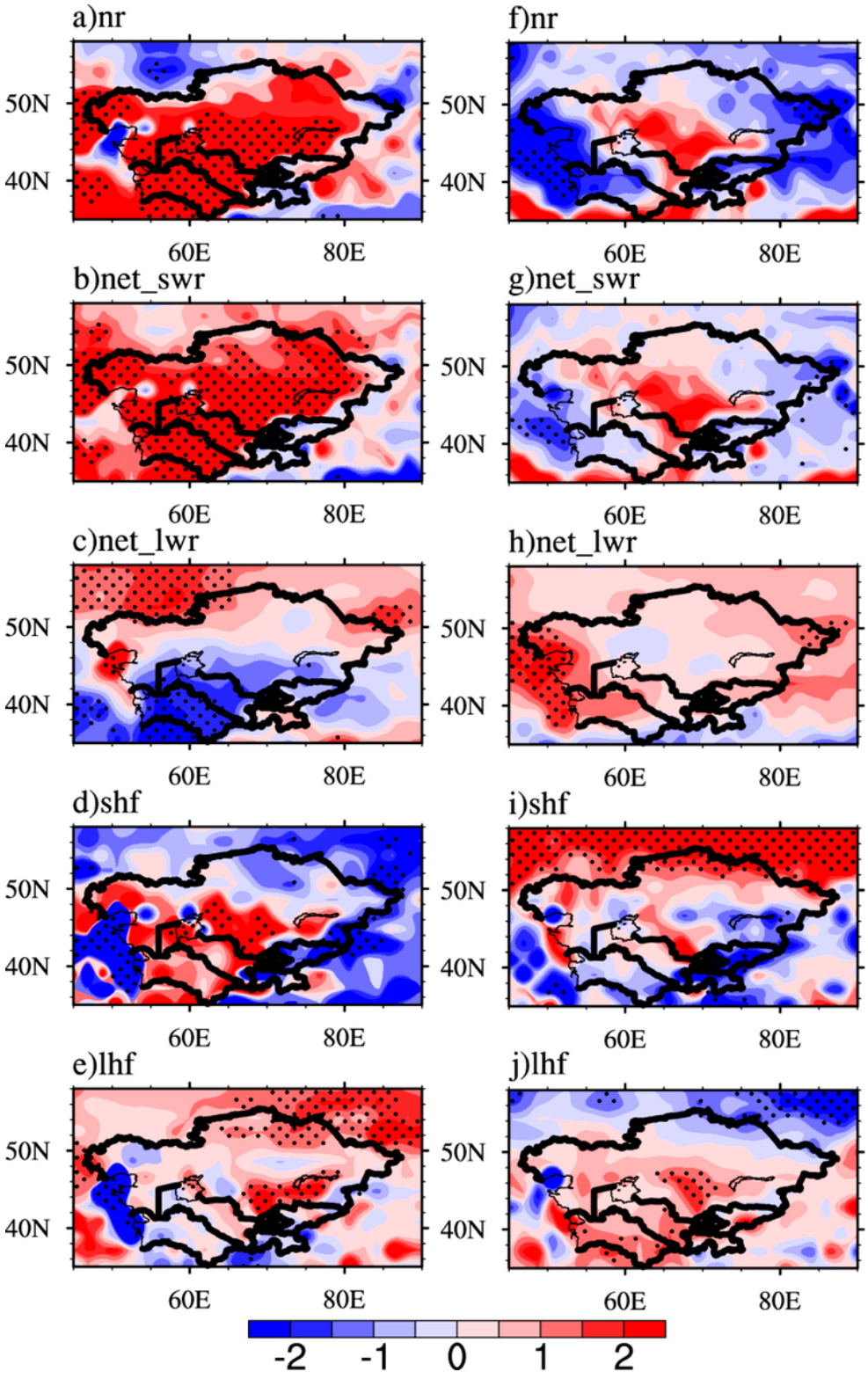

Figure 10

Regression maps for surface a, f net radiation, b, g net shortwave radiation, c, h net longwave radiation, d, i sensible heat flux and e, j latent heat flux based on the EOF1 and EOF2 time series of the anomalous CSAT over Central Asia for the period of 1979-2016 (The black dots indicate regions where the regression correlations are exceeding the 95% confidence level). Net radiation (net shortwave radiation plus net longwave radiation). Net shortwave radiation (net downward shortwave radiation minus net upward

shortwave radiation), and net longwave radiation (net downward longwave radiation minus net upward longwave radiation. The Central Asia is marked by the black lines). Note: The designations employed and the presentation of the material on this map do not imply the expression of any opinion whatsoever on the part of Research Square concerning the legal status of any country, territory, city or area or of its authorities, or concerning the delimitation of its frontiers or boundaries. This map has been provided by the authors.

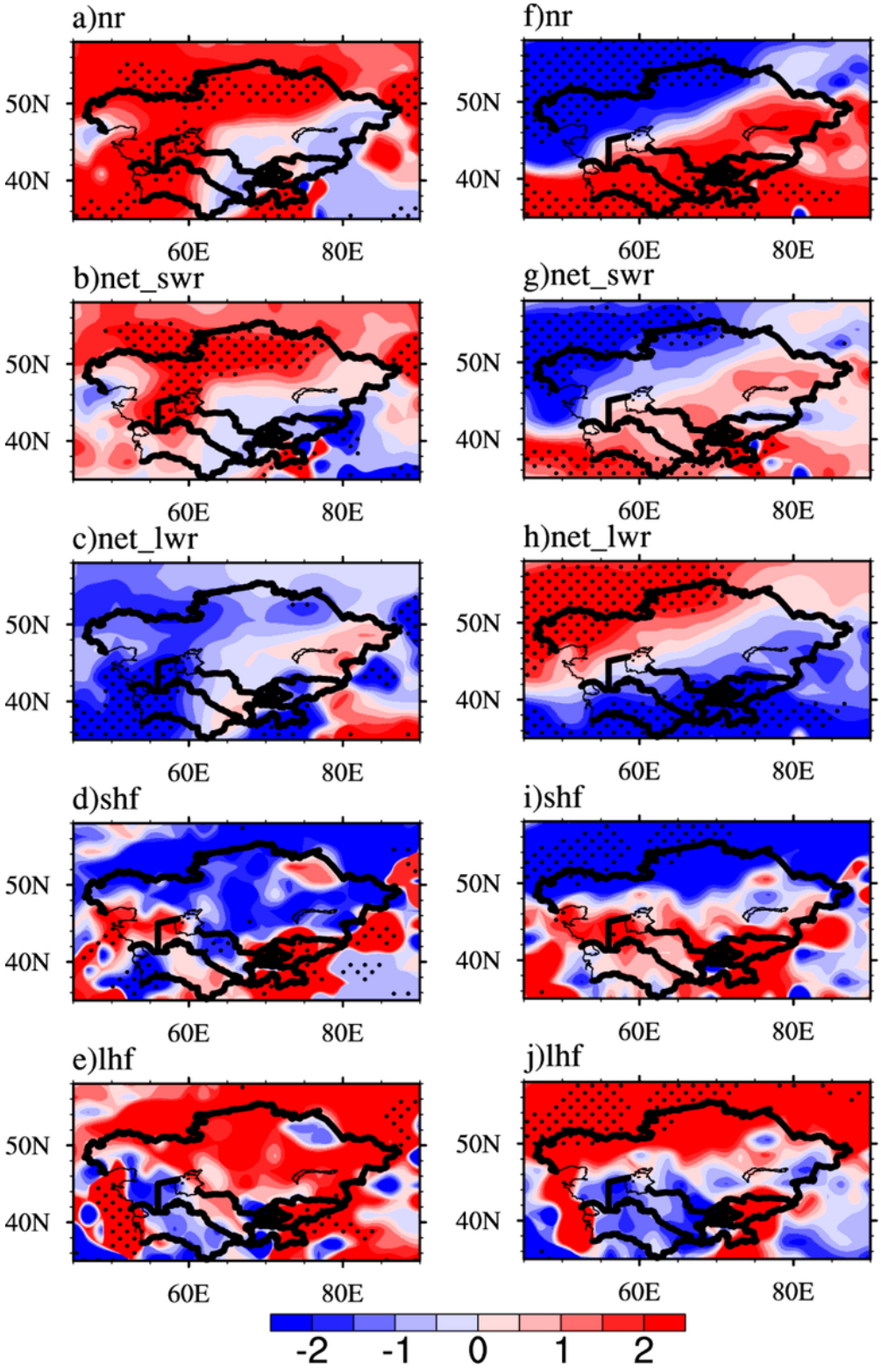

Figure 11

Same as Fig. 10, but for the anomalous WSAT over Central Asia. Note: The designations employed and the presentation of the material on this map do not imply the expression of any opinion whatsoever on the part of Research Square concerning the legal status of any country, territory, city or area or of its authorities, or concerning the delimitation of its frontiers or boundaries. This map has been provided by the authors.

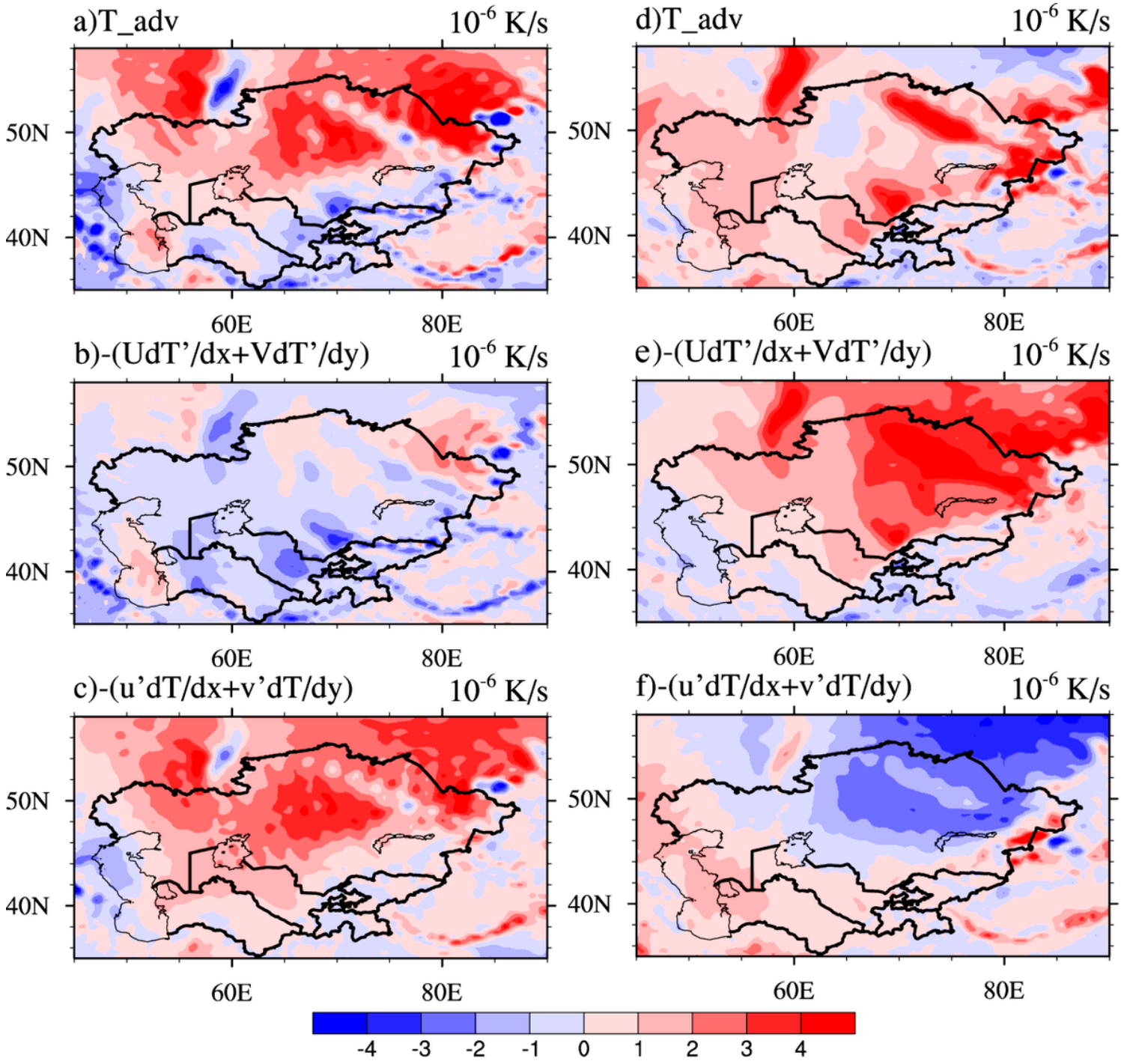

Figure 12

Spatial distributions of the 850-hPa air temperature advection obtained by regression on the EOF1 and EOF2 time series of the anomalous CSAT over Central Asia for the period of 1979-2016. The Central Asia is marked by the black lines. Note: The designations employed and the presentation of the material on

this map do not imply the expression of any opinion whatsoever on the part of Research Square concerning the legal status of any country, territory, city or area or of its authorities, or concerning the delimitation of its frontiers or boundaries. This map has been provided by the authors.

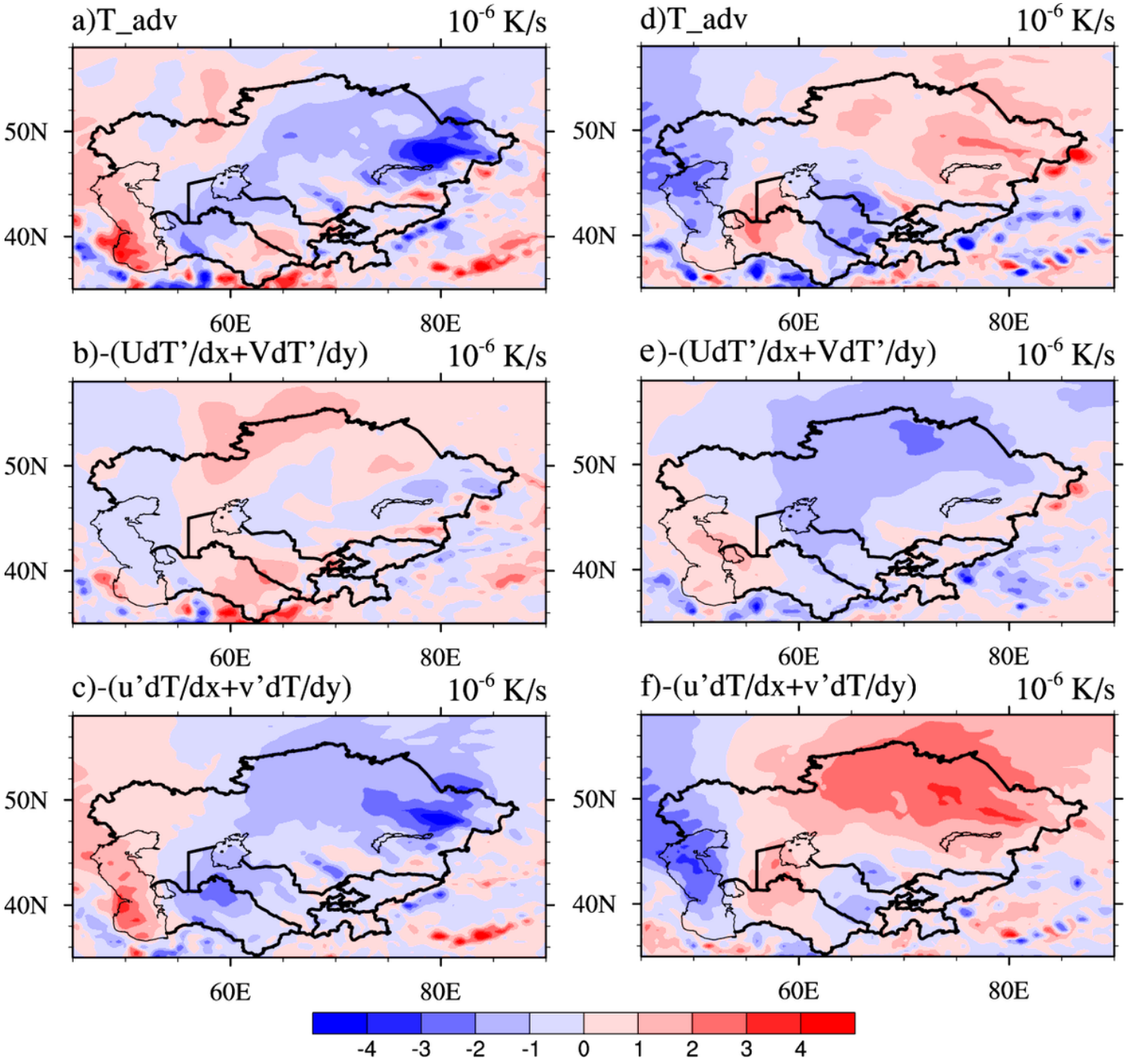

Figure 13

Same as Fig. 12, but for the anomalous WSAT over Central Asia. Note: The designations employed and the presentation of the material on this map do not imply the expression of any opinion whatsoever on the part of Research Square concerning the legal status of any country, territory, city or area or of its authorities, or concerning the delimitation of its frontiers or boundaries. This map has been provided by the authors.

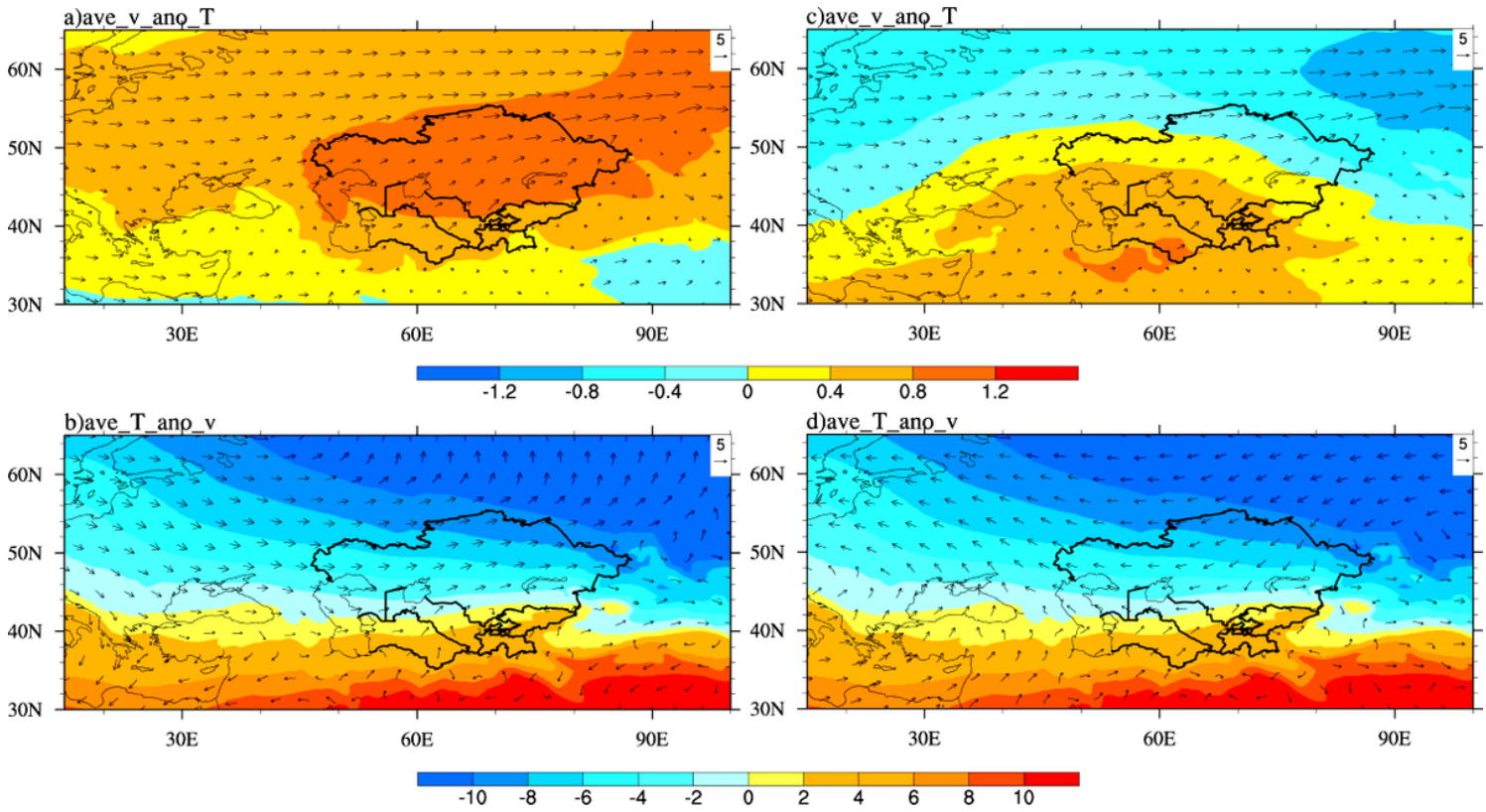

Figure 14

a, c The climatological mean winds (m·s -1; vectors; scale at upper-right corner) overlaid on temperature anomalies regression against the EOF1 and EOF2 time series of the anomalous CSAT over Central Asia for the period of 1979-2016. b, d The wind anomalies regression against the EOF1 and EOF2 time series of the anomalous CSAT over Central Asia for the period of 1979-2016 (m · s-1; vectors; scale at upper-right corner) overlaid on the climatological mean temperature at 850-hPa. The Central Asia is marked by the black lines. Note: The designations employed and the presentation of the material on this map do not imply the expression of any opinion whatsoever on the part of Research Square concerning the legal status of any country, territory, city or area or of its authorities, or concerning the delimitation of its frontiers or boundaries. This map has been provided by the authors.

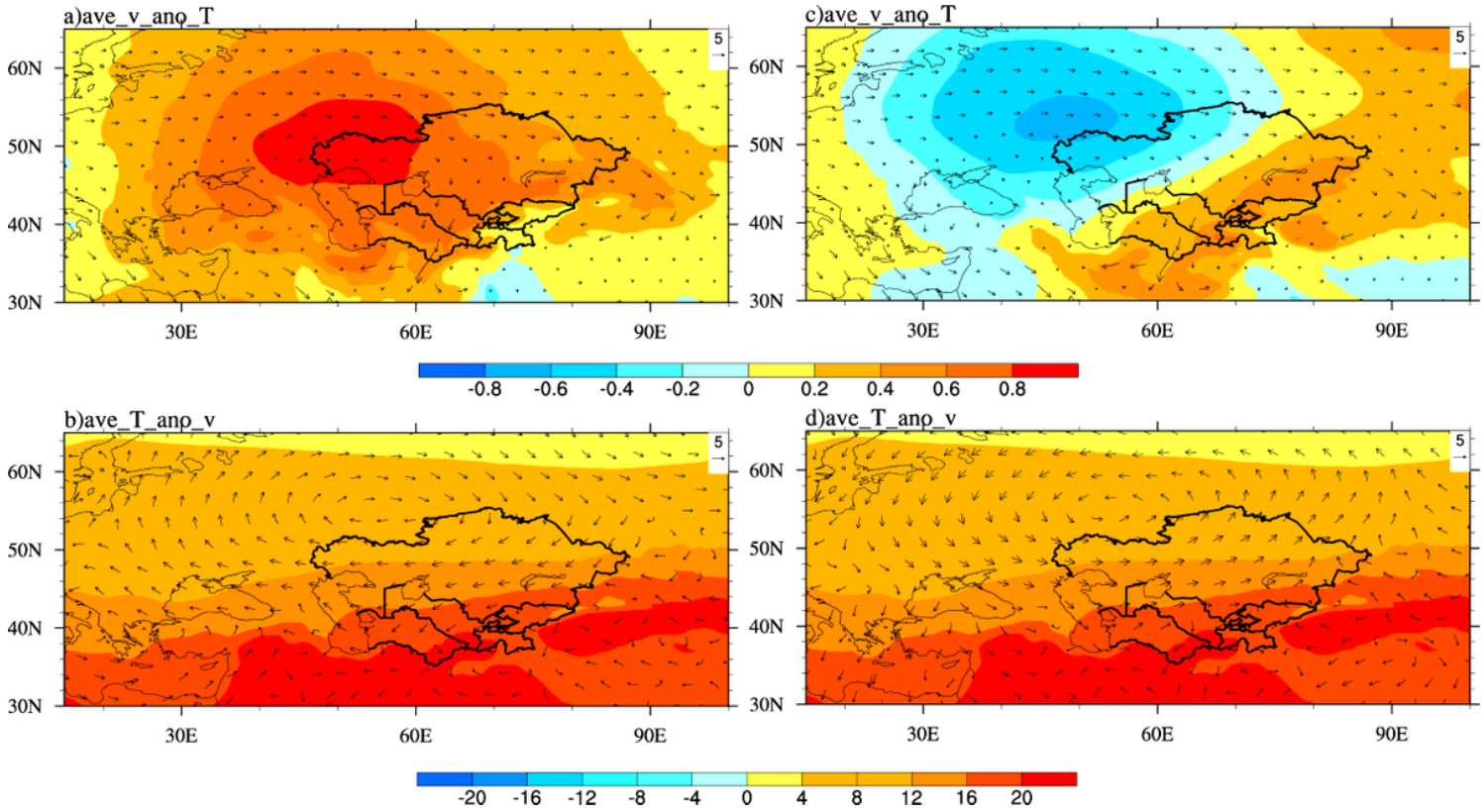

Figure 15

Same as Fig. 14, but for the anomalous WSAT over Central Asia. Note: The designations employed and the presentation of the material on this map do not imply the expression of any opinion whatsoever on the part of Research Square concerning the legal status of any country, territory, city or area or of its authorities, or concerning the delimitation of its frontiers or boundaries. This map has been provided by the authors.

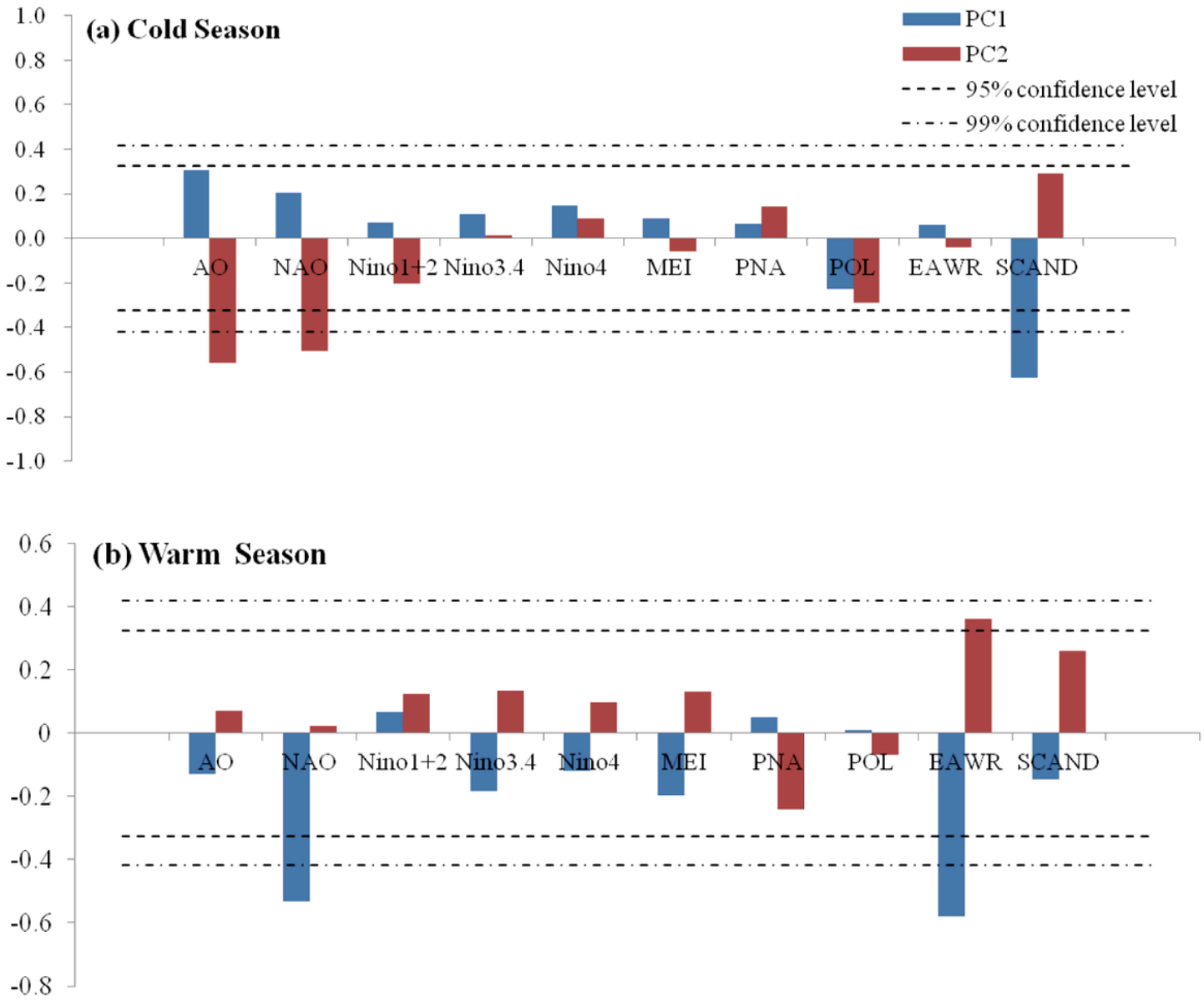

Figure 16

The correlation coefficients of the EOF1 and EOF2 time series of a the anomalous CSAT and b the anomalous WSAT over Central Asia with large-scale climate indices for the period of 1979-2016 (The dashed lines represent the 95% and 99% confidence levels).

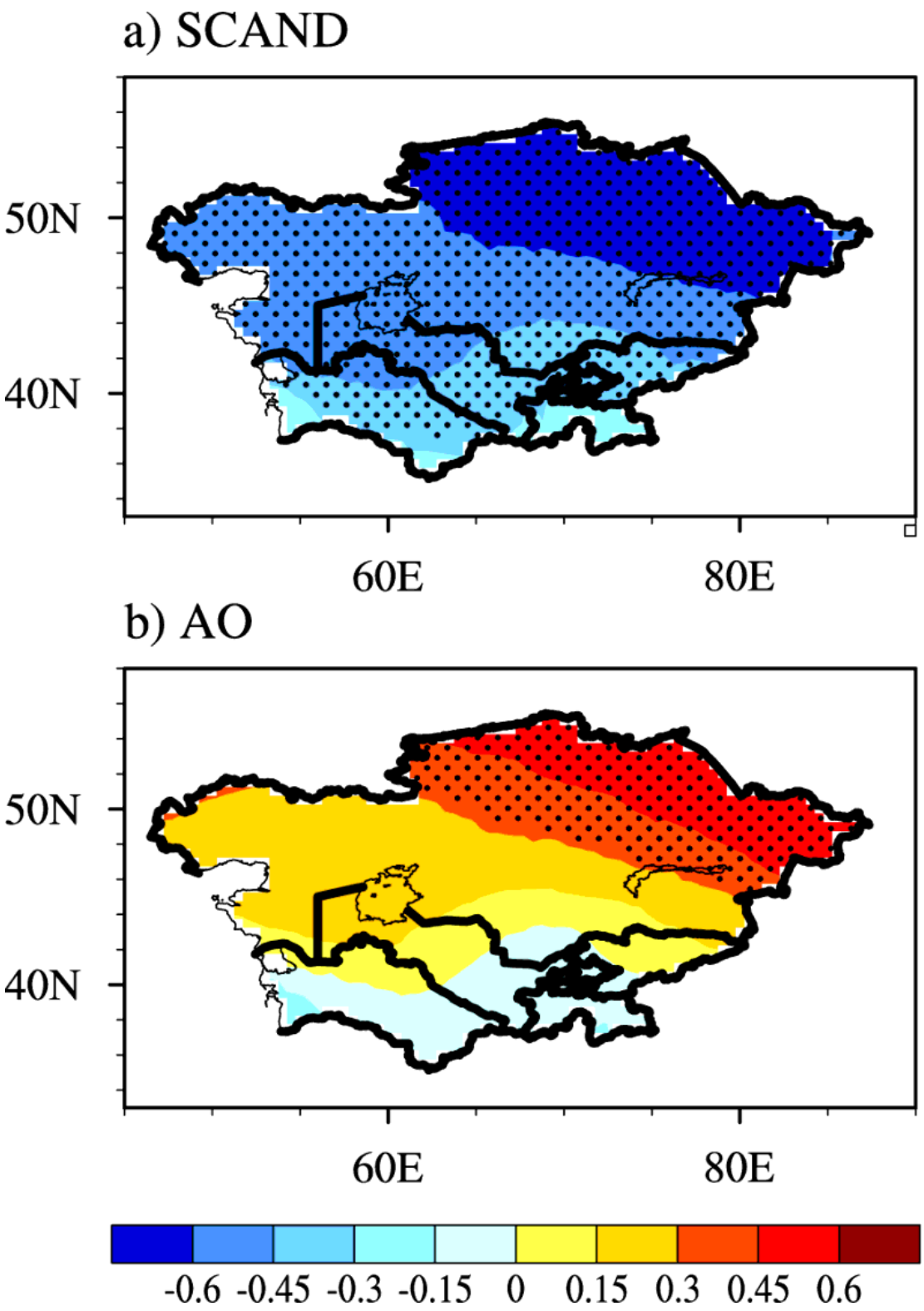

Figure 17

The spatial distributions of the correlation coefficients between the anomalous CSAT over Central Asia and a SCAND index; b AO index in the cold season (The black dots indicate the regions where the correlations are exceeding the 95% confidence level). Note: The designations employed and the presentation of the material on this map do not imply the expression of any opinion whatsoever on the part of Research Square concerning the legal status of any country, territory, city or area or of its

authorities, or concerning the delimitation of its frontiers or boundaries. This map has been provided by the authors.

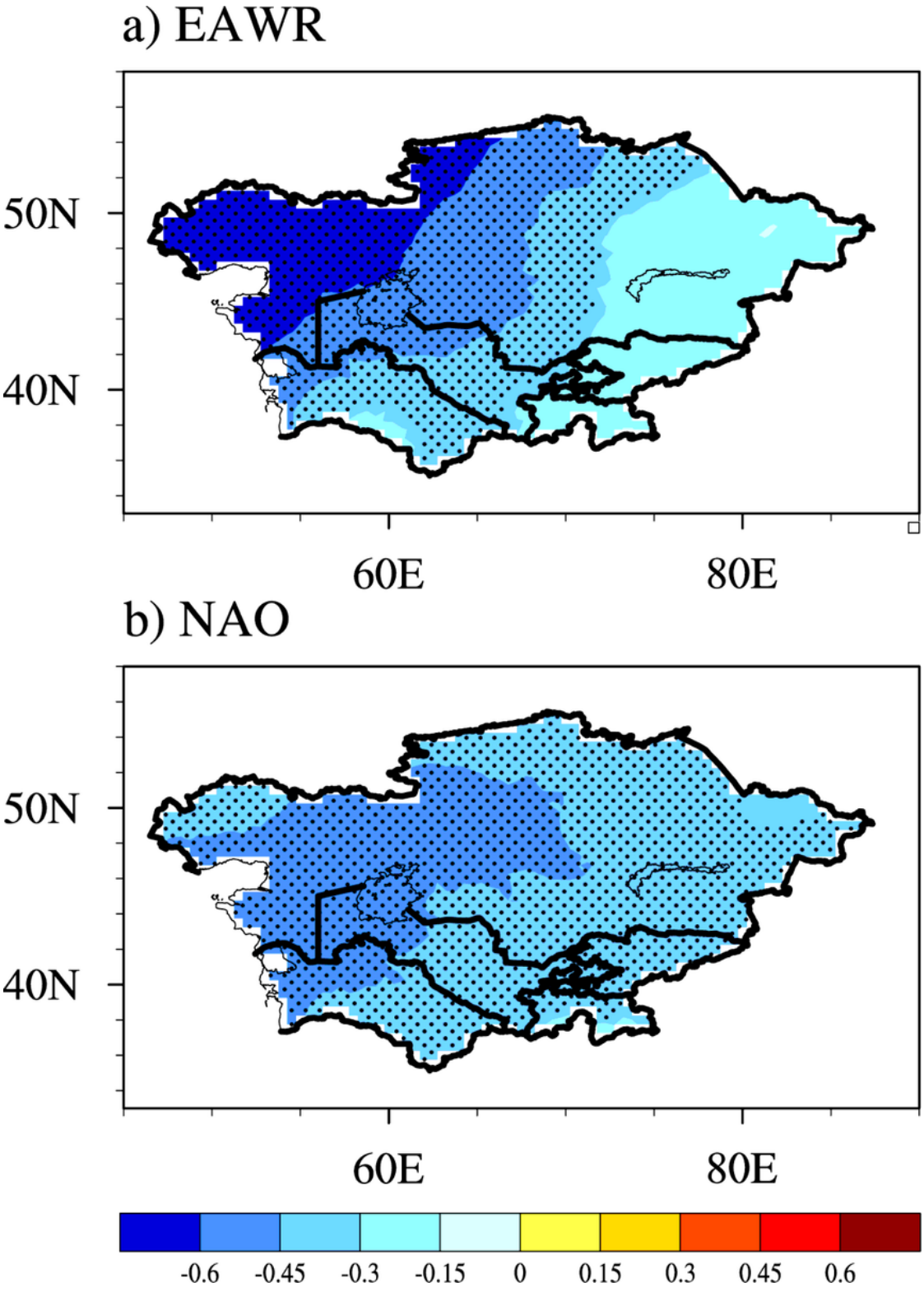

Figure 18

The spatial distributions of the correlation coefficients between the anomalous WSAT over Central Asia and a EAWR index; b NAO index in the warm season (The black dots indicate the region where the correlations are exceeding the 95% confidence level). Note: The designations employed and the

presentation of the material on this map do not imply the expression of any opinion whatsoever on the part of Research Square concerning the legal status of any country, territory, city or area or of its authorities, or concerning the delimitation of its frontiers or boundaries. This map has been provided by the authors.

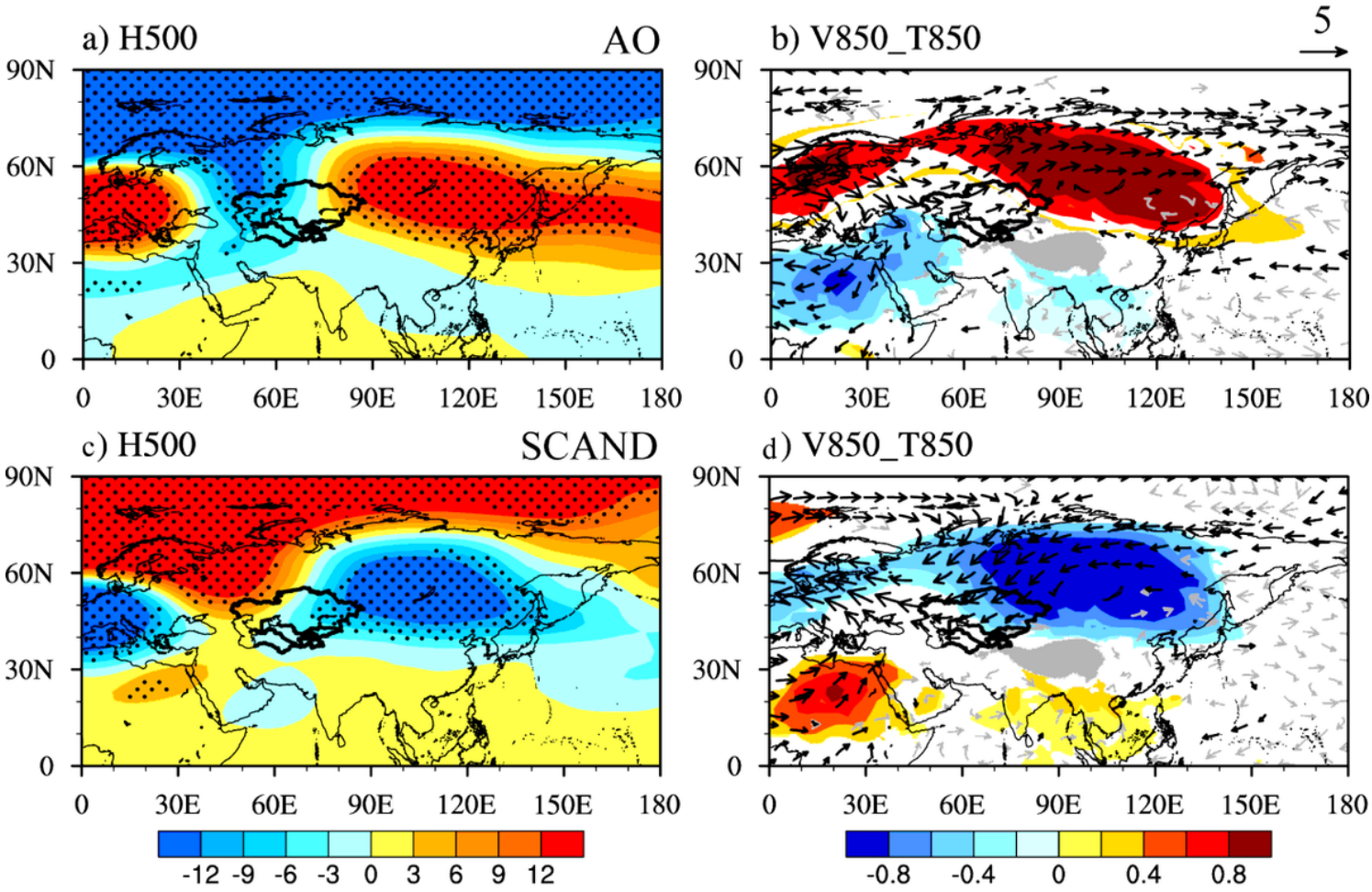

Figure 19

Regression maps of H500, V850 and T850 associated with the large-scale climate indices in the cold season for the period of 1979-2016: a, b AO index; c, d SCAND index; H500, V850 and T850 denote 500-hPa geopotential height, 850-hPa wind vector and 850-hPa air temperature (Black dots in a and c, the color shadows and black arrows in b and d indicate the 95% confidence levels based on a two-sided Student's t-test. The contour intervals of H500, V850 and T850 are 3gpm, 5m·s-1 and 0.2°C, respectively. The Central Asia is marked by the black lines). Note: The designations employed and the presentation of the material on this map do not imply the expression of any opinion whatsoever on the part of Research Square concerning the legal status of any country, territory, city or area or of its authorities, or concerning the delimitation of its frontiers or boundaries. This map has been provided by the authors.

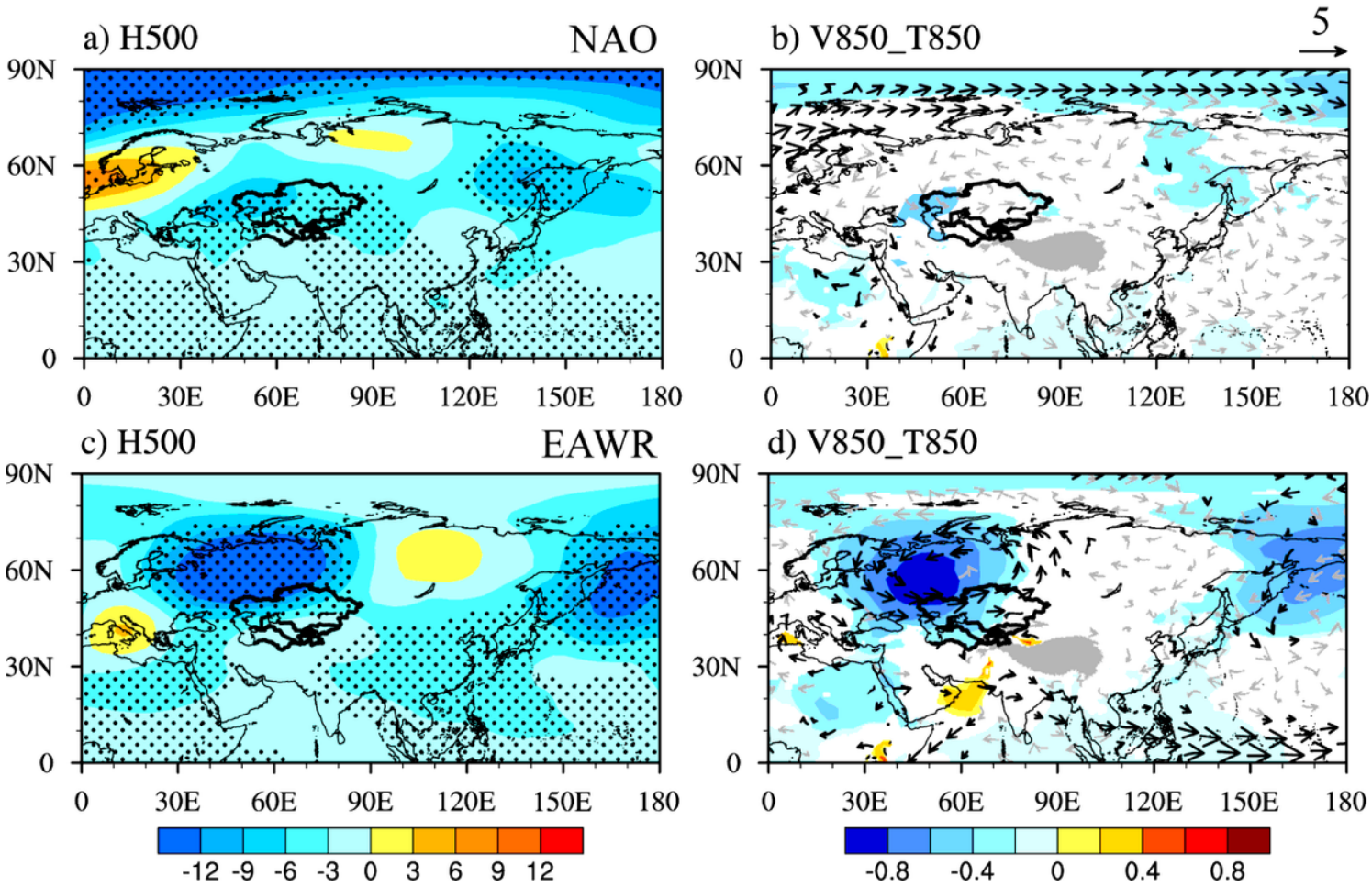

Figure 20

Regression map of H500, V850 and T850 associated with the large-scale climate indices in the warm season for the period of 1979-2016: a, b NAO index; c, d EAWR index; H500, V850 and T850 denote 500-hPa geopotential height, 850-hPa wind vector and 850-hPa air temperature (Black dots in a and c, the color shadows and black arrows in b and d indicate the 95% confidence levels based on a two-sided Student's t-test. The contour intervals of H500, V850 and T850 are 3gpm, 5m·s-1 and 0.2°C, respectively. The Central Asia is marked by the black lines). Note: The designations employed and the presentation of the material on this map do not imply the expression of any opinion whatsoever on the part of Research Square concerning the legal status of any country, territory, city or area or of its authorities, or concerning the delimitation of its frontiers or boundaries. This map has been provided by the authors.